# Methane, ethane, and propane production in Greenland ice core samples and a first isotopic characterization of excess methane

Michaela, Mühl[1], Jochen Schmitt[1], Barbara Seth[1], James E. Lee[2], Jon S. Edwards[3], Edward J. Brook[3], Thomas Blunier[4], Hubertus Fischer[1]

[1]Climate and Environmental Physics and Oeschger Centre for Climate Change Research, University of Bern, Bern, 3012, Switzerland
[2]Los Alamos National Laboratory, Earth Systems Observation, Los Alamos, NM 87545, USA
[3]College of Earth, Ocean, and Atmospheric Sciences, Oregon State University, Corvallis, OR 97331, USA
[4]Centre for Ice and Climate, Niels Bohr Institute, University of Copenhagen, Copenhagen, 2200, Denmark

*Correspondence to*: Michaela Mühl (michaela.muehl@unibe.ch)

**Abstract.** Air trapped in polar ice provides unique records of the past atmospheric composition ranging from key greenhouse gases such as methane ($CH_4$) to short-lived trace gases like ethane ($C_2H_6$) and propane ($C_3H_8$). Recently, the comparison of $CH_4$ records obtained using different extraction methods revealed disagreements in the $CH_4$ concentration for the last glacial in Greenland ice. Elevated methane levels were detected in dust-rich ice core sections measured discretely pointing to a process sensitive to the melt extraction technique. To shed light on the underlying mechanism, we performed targeted experiments and analyzed samples for methane and the short-chain alkanes ethane and propane covering the time interval from 12 to 42 kyears. Here, we report our findings of these elevated alkane concentrations, which scale linearly with the amount of mineral dust within the ice samples. The alkane production happens during the melt extraction step of the classic wet extraction technique and reaches 14 to 91 ppb of $CH_4$ excess in dusty ice samples. We document for the first time a co-production of excess methane, ethane, and propane, with the observed concentrations for ethane and propane exceeding their past atmospheric background at least by a factor of 10. Independent of the produced amounts, excess alkanes were produced in a fixed molar ratio of approximately 14:2:1, indicating a shared origin. The measured carbon isotopic signature of excess methane is (-47.0 ± 2.9) ‰ and its deuterium isotopic signature is (-326 ± 57) ‰ . With the co-production ratios of excess alkanes and the isotopic composition of excess methane we established a fingerprint that allows us to constrain potential formation processes. This fingerprint is not in line with a microbial origin. Moreover, an adsorption-desorption process of thermogenic gas on dust particles transported to Greenland appears not very likely. Instead, the alkane pattern appears to be indicative of abiotic decomposition of organic matter as found in soils and plant leaves.

## 1. Introduction

Atmospheric air entrapped in polar ice represents a unique archive of the past atmospheric composition including the concentration of greenhouse gases like carbon dioxide ($CO_2$), methane ($CH_4$), and nitrous oxide ($N_2O$) but also short-lived trace gases such as ethane ($C_2H_6$) and propane ($C_3H_8$). The ongoing anthropogenic increase in the atmospheric concentrations of these gases makes a detailed understanding of their preindustrial variations and biogeochemical cycling of paramount importance, and only polar ice cores are able to provide this information. However, to interpret reconstructions of the atmospheric composition from polar ice cores requires that archived atmospheric trace gases are not altered within the ice itself. Furthermore, the air must be extracted from the ice sample without altering the original composition. Thus,

70    the comparison of ice core records obtained using different extraction techniques and from

71    different ice cores requires careful consideration and interpretation.

72

73    Not all drill sites or specific time intervals are equally suitable to derive pristine atmospheric

74    trace gas records. For example, $CO_2$ data from Greenland ice are subject to $CO_2$ in situ

75    production due to impurities in the ice (Anklin et al., 1995; Smith et al., 1997). In situ

76    production is also observed for $N_2O$, for example, in glacial Antarctic ice core samples

77    characterized by higher dust content (Schilt et al., 2010). In contrast, $CH_4$ in polar ice cores, in

78    the absence of melt layers, was considered to be not affected by in situ processes. However,

79    more recent results from Greenland ice showing elevated $CH_4$ concentrations in glacial dust-

80    rich ice (Lee et al., 2020) and high amplitude $CH_4$ spikes in Holocene ice (Rhodes et al., 2013,

81    2016) question this assumption.

82

83    This becomes especially worrisome as atmospheric methane shows a significant North-South

84    gradient, reflecting the predominance of Northern Hemisphere sources. Ice cores from

85    Greenland and Antarctica have been used to quantify this Inter-Polar Difference (IPD) in past

86    $CH_4$ concentrations (Chappellaz et al., 1997; Baumgartner et al., 2012, Beck et al., 2018) to

87    derive the relative contribution of Northern and Southern hemispheric sources to the overall

88    $CH_4$ changes. The Holocene IPD is on the order of several tens of ppb, i.e., one order of

89    magnitude smaller than the past atmospheric $CH_4$ concentration. Thus, any small $CH_4$ bias on

90    the order of a few ppb to tens of ppb strongly impacts the conclusions drawn from this IPD,

91    while the influence on the total radiative forcing by such small biases is negligible. In summary,

92    existing results of $CH_4$ concentrations from Greenland and Antarctic ice cores have to be

93    carefully scrutinized for such effects.

94

95    A first step in this direction has been made in previous work by Lee et al. (2020), for example

96    by comparing $CH_4$ records derived using different measurement techniques. Past $CH_4$

97    concentrations ([$CH_4$]) are retrieved by measurements of Greenland and Antarctic ice cores

98    using traditional discrete and relatively new continuous melt extraction techniques. While

99    discrete ice measurements deliver one single value for each sample, Continuous Flow Analysis

100   (CFA) gradually melts a thin stick of the ice core providing a continuous record for this section.

101   Although in both techniques the ice sample is melted, the CFA technique separates air from the

102   meltwater stream in about 1-2 min providing only a short time for any reaction in the water,

103   while for the discrete technique the contact time is typically 15-30 min. Comparing [$CH_4$]

histories from several Greenland ice cores measured discretely (NGRIP, GISP2, GRIP) with the continuous Greenland NEEM and the continuous Antarctic WAIS records over the last glacial period, higher [CH$_4$] can be found in the discrete Greenland measurements for specific time intervals (Lee et al., 2020; Fig. 1 therein), where dust concentrations are especially high.

Looking at the NGRIP methane hydrogen isotope ($\delta$D-CH$_4$) record (Bock et al., 2010b), which was also measured with a discrete melt extraction technique (Bock et al., 2010a), it turns out that in the high dust ice sections, the isotopic values are also affected. Several negative $\delta$D-CH$_4$ excursions with a maximum depletion of 16 ‰ (permil) prior to the onset of Dansgaard-Oeschger (DO) event 8 were identified (Bock et al., 2010b). At the time of that publication there was no straightforward explanation for these $\delta$D-CH$_4$ depletions during times of a relatively stable climate. Using ice from Antarctica, much smaller $\delta$D-CH$_4$ variations (3-4 ‰) during this interval were found in measurements performed at the University of Bern (unpublished data), again questioning the atmospheric origin of these $\delta$D-CH$_4$ depletions prior to the DO onset.

All these observations in Greenland ice give reason to assume that a hitherto unknown process exists that produces or releases additional methane in some time intervals in Greenland ice cores (from here on referred to as "excess methane" or CH$_{4(xs)}$). This process is related to the extraction technique (only found in records obtained by discrete melt extractions) and has only been observed in glacial Greenland ice with high mineral dust concentrations.

A first attempt to characterize CH$_{4(xs)}$ was made by Lee et al. (2020) who analyzed [CH$_4$] in discrete ice samples with different impurity composition and concentration from several ice cores (GISP2, NEEM, WAIS, SPICE) using a multiple melt-refreeze technique. They were able to quantify CH$_{4(xs)}$ contributions of up to 30-40 ppb for Greenland samples. Sequential melt-refreeze extractions showed that the process leading to CH$_{4(xs)}$ is slow and not completed during the first melt-refreeze cycle (i.e., within around 30 min). A set of samples was analyzed with the admixture of a HgCl$_2$ solution to suppress microbial activity in the meltwater. No difference in the measured [CH$_4$] was observed between the poisoned samples and replicates without HgCl$_2$, excluding a microbial CH$_4$ production after melting. In addition, Lee et al. (2020) used the NGRIP [CH$_4$] (Baumgartner et al., 2014) and $\delta$D-CH$_4$ records (Bock et al., 2010b) to estimate the deuterium isotopic signature of the CH$_{4(xs)}$. Assuming a two-component mixture

137     of atmospheric methane and excess methane, their model led to a best estimate of (-293 ± 31)

138     ‰ for $\delta$D- $CH_{4(xs)}$.

139

140     A straightforward explanation for $CH_{4(xs)}$ may be that $CH_4$ is either produced in the meltwater,

141     or it was produced beforehand and only released during the melt extraction. With respect to

142     that, Lee et al. (2020) reviewed several mechanisms that could account for the observed

143     variations in Greenland ice core records. None perfectly matched all their observations but

144     lastly, three of the proposed mechanisms were short-listed by Lee et al. (2020): (1) an

145     adsorption process on dust particles prior to the deposition on the ice sheet; (2) an in situ

146     production in the ice; or (3) an abiotic reaction during melt extraction.

147

148     Here we resume the work by Lee et al. (2020) and shed more light upon the potential formation

149     processes using a targeted and more comprehensive study to quantify $CH_{4(xs)}$. We analyzed

150     specific NGRIP and GRIP ice core samples discretely with two different wet extraction

151     systems. With our $\delta^{13}$C-$CH_4$ device we are able to measure [methane], [ethane], [propane], and

152     $\delta^{13}$C-$CH_4$ on a single ice sample in two subsequent extractions. With our second device we add

153     experimental information on $\delta$D-$CH_4$. In Sect. 2, we provide information on our sampling

154     strategy and measurement techniques. With our new experimental results, presented in Sect. 3,

155     we provide quantitative data for $CH_{4(xs)}$ in NGRIP and GRIP samples and extend our

156     observations to other "excess alkanes" (ethane and propane), which are revealed to be co-

157     produced during the excess $CH_4$ production. The observed molar ratios between methane,

158     ethane, and propane are evaluated and their relation to the abundance of mineral dust ($Ca^{2+}$)

159     within the ice samples is quantified. A 2nd extraction of the meltwater enables us to estimate

160     the temporal dynamics of excess alkane production. Using a Keeling-plot approach to our

161     isotopic results, we calculate the carbon and deuterium isotopic signature of excess $CH_4$ ($\delta^{13}$C-

162     $CH_{4(xs)}$ and $\delta$D-$CH_{4(xs)}$). Based on our new and improved observations, we finally come back

163     to the discussion of the hypotheses proposed by Lee et al. (2020) in Sect. 4 and offer potential

164     mechanisms that could explain the excess alkanes in ice core samples. For readers not interested

165     in all the experimental details, we recommend to jump straight to Sect. 4 to see the discussion.

166

167

168

## 2. Ice core samples and measurements

### 2.1 Ice core samples

Mixing ratios of alkanes (methane, ethane, and propane) and the stable carbon ($\delta^{13}$C-CH$_4$) and hydrogen ($\delta$D-CH$_4$) isotope ratios of methane were measured on ice core samples from the North Greenland Ice Core Project (NGRIP) ice core. For this study, 19 NGRIP ice core samples were measured for $\delta^{13}$C-CH$_4$ and alkane concentrations and nine NGRIP ice samples for $\delta$D-CH$_4$ covering the depth between 1795.84 m and 1933.25 m. The NGRIP samples are from the late glacial Marine Isotope Stages (MIS) 3 and 2 (22.6 to 30.6 kyears BP). These time intervals are characterized by sharp atmospheric CH$_4$ increases in parallel to rapid warmings, the so-called Dansgaard-Oeschger events, but we mostly sampled intervals with stable CH$_4$ concentrations. From the same time period, we also investigate measurements of 41 NGRIP and 12 GRIP ice core samples which were carried out in 2011 and 2018, respectively, and which have not previously been published. See Fig. 1 for an overview of all analyzed NGRIP and GRIP ice core samples over time.

We also included 22 ice core samples from the European Project for Ice Coring in Antarctica (EPICA) ice core from Dome C (MIS 4), which are not affected by a measurable excess CH$_4$ production and which we use as long-term monitoring ice for the system performance and to quantify the blank contribution of the analytical system (see Appendix B).

The late glacial period, which includes the age of most of the measured NGRIP samples, is characterized by an overall high impurity and dust content and low atmospheric methane concentrations. For our analysis, we have selected ice core bags (where for NGRIP and GRIP ice cores, a bag is a 55 cm long ice core section) in which we expect the same atmospheric CH$_4$ concentration but see a high range of mineral dust content (Ca$^{2+}$). In this way, we can compare neighbouring samples with the same low stadial CH$_4$ levels due to stable atmospheric concentrations and temporal smoothing by the slow bubble enclosure process but are expected to vary in measured concentrations due to contributions of excess alkanes. Ca$^{2+}$ content across our NGRIP samples ranges from 307 ng/g to 1311 ng/g. This sample selection is critical to quantify the isotope signature of the CH$_{4(xs)}$ produced using the Keeling-plot approach (Keeling, 1958). The underlying assumptions of this mass balance approach are (1) that there is only a two-component mixture (atmospheric methane and excess methane) and (2) that the isotopic ratio of the mixture changes only by a varying input of the second source (CH$_{4(xs)}$).

203  To select the samples, we use high-resolution mineral dust records measured using an Abakus
204  laser attenuation device (Klotz, Germany) for particulate dust (Ruth et al., 2003) as well as $Ca^{2+}$
205  concentrations (Erhardt et al., 2022) as dissolved mineral dust tracer derived from the Bern
206  Continuous Flow Analysis System (Kaufmann et al., 2008). In principle, particulate dust and
207  the soluble dust tracer $Ca^{2+}$ are strongly correlated. However, depending on acidity of the ice
208  (mainly due to $H_2SO_4$ and $HNO_3$), variable amounts of $CaCO_3$ are converted into soluble $CaSO_4$
209  and $Ca(NO_3)_2$, leading to a variable $Ca^{2+}$/ dust ratio (Legrand and Delmas, 1988). As an
210  example, Fig. 2 shows the $Ca^{2+}$ and mineral dust concentration of the NGRIP bag 3292 which
211  we used to select the individual samples and the relevant parameters measured for each sample
212  of this bag. The data overview for all other measured NGRIP bags can be found in Appendix
213  A.
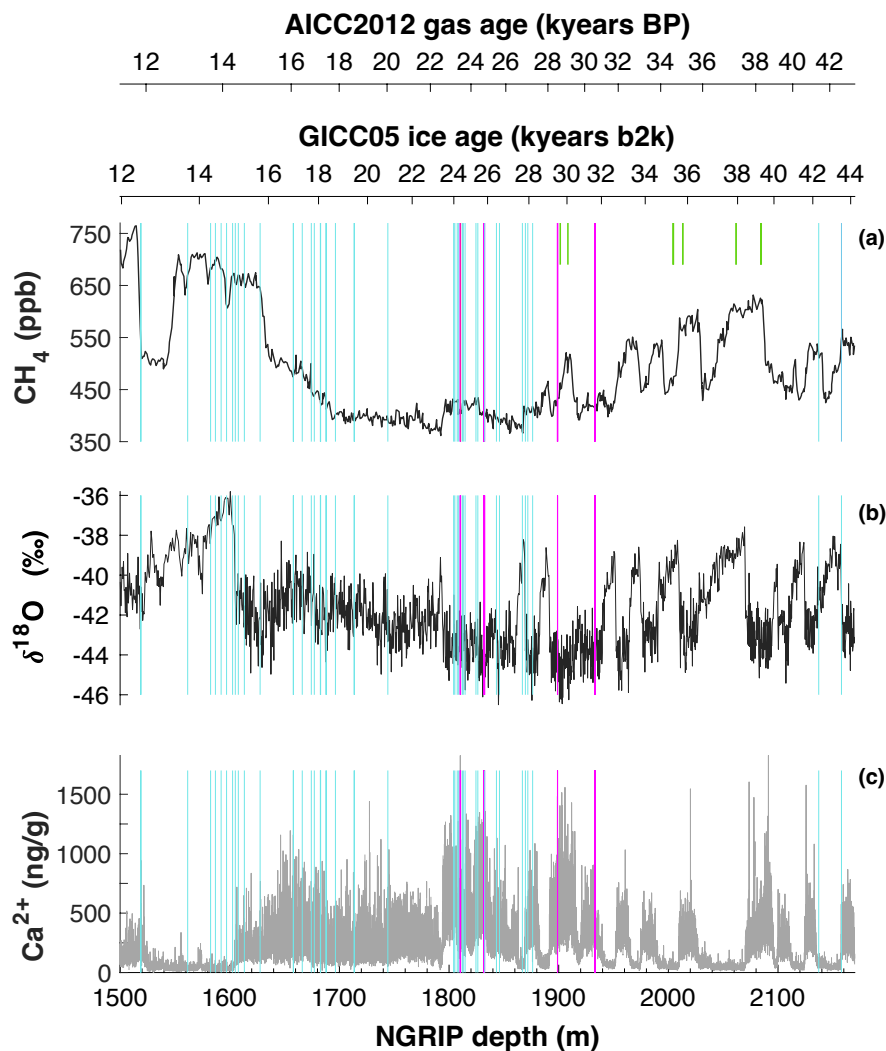
214
215  Figure 1: **Overview of the analyzed NGRIP and GRIP samples over time.** All analyzed NGRIP and GRIP ice
216  core samples are indicated on the NGRIP depth (m) on the bottom axis. To indicate an age for the gas and ice
217  records both the AICC2012 gas age (kyears BP) and the GICC05 ice age (kyears b2k) scale are provided on the
218  upper axes. Note that for the purpose of describing the excess $CH_4$ production in a certain ice sample the age is
219  not important and we provide all records on depths throughout this manuscript. NGRIP samples measured from

the five main bags (3292, 3331 & 3332, 3453, 3515) for the Keeling-plot approach are indicated with vertical lines
in pink, NGRIP samples measured in 2011 and individual NGRIP ice core samples measured in 2019-2020 (not
included in the Keeling-plot analyses) in turquoise, and GRIP ice core samples in green. **(a)** [CH₄] record measured
by wet extraction from NGRIP samples from Baumgartner et al. (2012, 2014). **(b)** $\delta^{18}$O record from North
Greenland Ice Core Project members (2004). **(c)** $Ca^{2+}$ record from Erhardt et al. (2022).
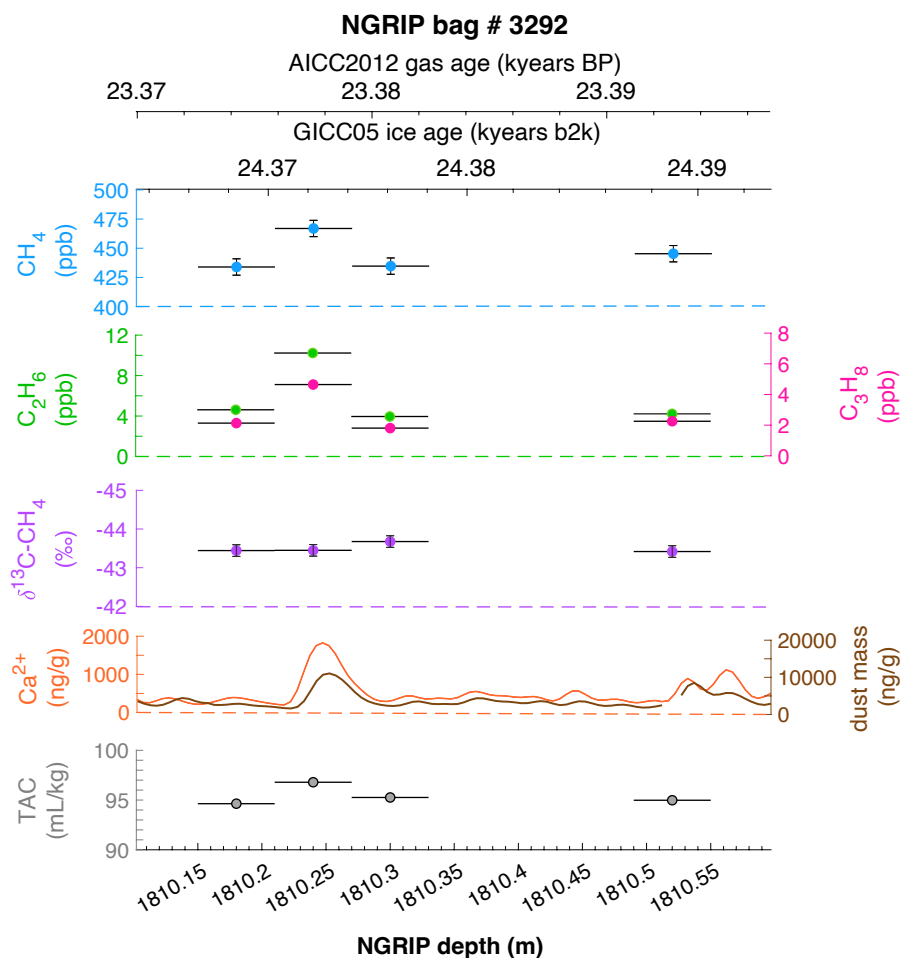
Figure 2: **Detailed data overview for NGRIP bag 3292.** Bag-specific overview of several parameters measured
for each sample in this bag at a given depth: methane, ethane, propane, $Ca^{2+}$, mineral dust mass, TAC (Total Air
Content), $\delta^{13}$C-CH₄. At the top the AICC2012 gas age (upper top axis) and the GICC05 ice age (lower top axis) of
the respective depth are indicated. The mineral dust record is taken from Ruth et al. (2003), the $Ca^{2+}$ record from
Erhardt et al. (2022). The data overview for all further measured NGRIP bags can be found in Appendix A.

## 2.2 CH₄, C₂H₆, C₃H₈ and $\delta^{13}$C-CH₄ Analysis of Ice Core Samples

The short-chain alkanes and $\delta^{13}$C-CH₄ were measured at the University of Bern using the

discrete wet extraction technique described in Schmitt et al. (2014). With this method, it is

possible to measure mixing ratios of methane, ethane, and propane as well as the methane

carbon isotopic signature and other trace gases on a single ice core sample of about 150 g.

Briefly, ice core samples are placed in a glass vessel locked by a stainless-steel flange which is

attached to the vacuum line to evacuate laboratory air (see Fig. 3, step a). Before melting the

243 ice sample, the leak tightness of the vacuum extraction line is tested with a so-called He blank.

244 The ice sample is then melted under vacuum with the help of infrared radiation for ~35 min to

245 release the enclosed air (step b). The released air is continuously removed from the sample

246 vessel by a pressure gradient towards an adsorbing AirTrap (activated carbon), collecting all

247 relevant air components at -180°C. After melting is completed, the temperature of the meltwater

248 is stabilized close to 0°C, but does not refreeze again. Afterwards, He is sparged with 4 mL/min

249 at standard temperature and pressure (equivalent to 100-400 mL at the varying low pressure in

250 the headspace) through the melt water for ~14 min through a capillary at the bottom of the

251 vessel to transfer any remnant gas species dissolved in the melt water onto the AirTrap (step c).

252 The sample vessel is then isolated by closing the inlet and outlet valves (step d). Consecutively,

253 the AirTrap is warmed up in two steps to first remove $N_2$ and $O_2$ and in a second step to release

254 the gases of interest which are then sent after a cryofocus step to the gas chromatograph (GC)

255 for separation and quantification using an isotope ratio mass spectrometer (Isoprime 100,

256 Elementar).

257

258 Precision of this method for $CH_4$ is about 8 ppb and 0.1 ‰ for $\delta^{13}C$-$CH_4$ based on the

259 reproducibility of the 1st extraction of ice core samples where isotopic data are expressed using

260 the $\delta$ notation on the international Vienna Pee Dee Belemnite (VPDB) scale. For $C_2H_6$, the

261 precision is 0.02 ppb or 1 %, for $C_3H_8$, 0.03 ppb or 5 % (whatever is higher) based on the

262 reproducibility of standard air samples which are by definition not subject to excess production

263 (Schmitt et al., 2014). Blank levels for these species based on melted artificial (gas-free) ice

264 samples are 1-2 ppb for $CH_4$, 0.3 ppb for $C_2H_6$ and 0.2 ppb for $C_3H_8$ (Schmitt et al., 2014),

265 which are below the values measured on Antarctic ice, where excess production is minimal

266 compared to glacial Greenland samples (see Appendix B for details).

267

268 With their experimental investigations, Lee et al. (2020) were already able to demonstrate that

269 production/ release of $CH_{4(xs)}$ is time-dependent. We therefore conclude that this process does

270 not have to be completed in the time available for the gas extraction described above. We

271 continued the analyses of excess alkane production with an additional extraction step (here

272 referred to as 2nd extraction, steps d-g in Fig. 3) following the normal ice extraction routine.

273 After all sample air is collected in the 1st extraction, the meltwater is left in the isolated sample

274 vessel (the vessel is closed and not connected to the carbon trap) and held at temperatures close

275 to 0°C for ~100 min (step d). After this "waiting time" of ~100 min, He is purged through the

276 meltwater for ~24 min to extract the gases that have been accumulated during this time interval

simulating the extraction time of the 1st extraction, followed by another ~14 min of He purging to mimic the last step of the ice extraction when the sample had completely melted (step f). The gases from this 2nd extraction are collected and measured following the same trapping and separation steps as in the 1st extraction. Note that the procedure of the 2nd extraction can be repeated any number of times (e.g. 3rd extraction).

The amount of gases that we obtain from the 1st extraction comprises the atmospheric amount, a possible contribution by in situ production, and a potential time-dependent production/release in the meltwater (*in extractu*). The 2nd extraction, however, targets only the *in extractu* fraction. The system blank for the 2nd extraction was estimated using the 2nd extraction of Antarctic ice (Talos Dome, EDC) and were 2 ppb, 0.3 ppb and 0.3 ppb for $CH_4$, $C_2H_6$ and $C_3H_8$, respectively, assuming an ice core sample air volume of 14 mL at standard temperature and pressure, which is the typical ice sample size of 150 g with a total air content of 0.09 mL/g. For $CH_4$ this is < 1% of the amount of extracted species in the 1st extraction of glacial Greenland ice. Due to the small amount of $CH_4$ analyzed in this 2nd extraction (about a factor of 20 to 50 less than for an ice core sample) the precision for the $\delta^{13}C$ analysis is much lower than for the 1st (ice sample) extraction and we estimate the precision of $\delta^{13}C$-$CH_4$ to 2 ‰ and for [$CH_4$] to be 2 ppb or 10 % (based on the reproducibility of 2nd extractions of Antarctic EDC samples). For $C_2H_6$ and $C_3H_8$, the precision is comparable to the 1st extraction. Note that throughout the manuscript we do not perform blank corrections (neither for the measured alkane concentrations nor for the isotopic values). The only exception is for the calculation of the temporal dynamics of excess ethane production (see Appendix C) as the blank contribution would otherwise bias the samples with low $Ca^{2+}$ content.
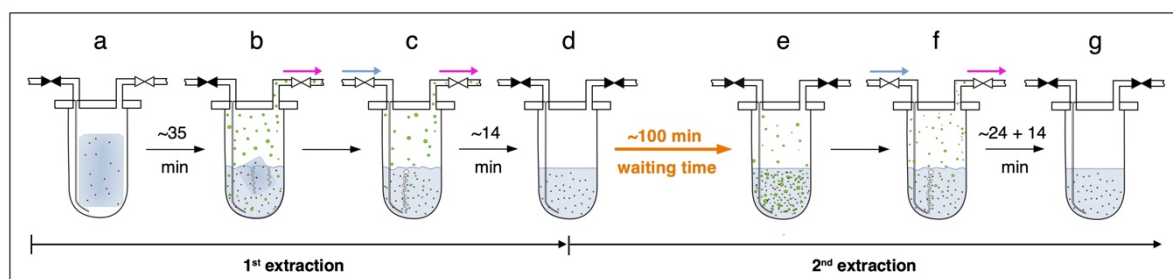
*Figure 3: S***equential steps (a-g) happening in the ice core sample vessel during the 1st and the 2nd extraction in the $\delta^{13}C$-$CH_4$ extraction line**. Scheme illustrates the subsequent steps as described in detail in the text. Brownish spots indicate dust particles in the ice/ meltwater. Green circles indicate gas species (methane, ethane, and propane) in the meltwater or in the headspace of the vessel. Closed valves are indicated in black, open vales in white. Blue arrows indicate the He flow through the inlet capillary into the sample vessel, pink arrows indicate the flow direction from the sample vessel towards the AirTrap.

### 2.3 $\delta$D-CH$_4$ Analysis of Ice Core Samples

All $\delta$D-CH$_4$ data presented here were measured at the University of Bern using the discrete wet extraction technique described in Bock et al. (2010a, 2014). This $\delta$D-CH$_4$ device allows to measure the concentration of methane and its deuterium isotopic signature ($\delta$D-CH$_4$) on a single ice core sample of about 300 g.

Briefly, ice core samples are melted after evacuation of the headspace using a warm water bath at 40°C for 25-30 min to release the enclosed air into the sample vessel headspace. Once all the ice is melted, the warm water bath is replaced by an ice-water bath to keep the meltwater temperature and water vapor pressure low but without refreezing. In contrast to the $\delta^{13}$C-CH$_4$ method, the inlet and outlet valves are closed during the melting process. The released air leads to an increased pressure in the sample vessel headspace enhancing the solubility of gases in water. After the melting is complete, the inlet and outlet valves are opened and He is purged for ~40 min with a flow of 360 mL/min to transfer the accumulated air in the headspace and bubble He through the meltwater to strip dissolved gases. Just like for the $\delta^{13}$C-CH$_4$ method, the air is collected on an activated carbon trap followed by further purification steps including GC separation. Note that compared to the $\delta^{13}$C-CH$_4$ device, we performed only one extraction with the $\delta$D-CH$_4$ device.

For both methods, we assume that the time for an *in extractu* production during the ice extraction procedure starts with the first presence of meltwater until He purging is stopped. Note that this time is considerably longer for the $\delta$D-CH$_4$ analysis (~60 min) compared to the time of the 1$^{st}$ extraction in the $\delta^{13}$C-CH$_4$ analysis (~35 min).

Using this method we can measure [CH$_4$] and $\delta$D-CH$_4$ with a precision of about 15 ppb and 3 ‰ (based on standard ice sample measurements), where isotopic data are expressed using the $\delta$ notation on the international Standard Mean Ocean Water (SMOW) scale.

### 3. Characterization of excess alkanes in ice cores

### 3.1 Methane, ethane, propane concentrations

As described in detail in Sect. 2.2 a full ice sample measurement includes the regular ice sample extraction (1$^{st}$ extraction) and, after the waiting time of ~100 min, a 2$^{nd}$ gas extraction in the meltwater. Gas from the 1$^{st}$ extraction comprises atmospheric air, a possible contribution from

344 in situ production, a potential time-dependent contribution by an *in extractu* process, and any
345 contribution from the device itself (blank). For the gas species discussed here (methane, ethane,
346 propane), these individual fractions are very different in magnitude. For polar ice core samples,
347 the atmospheric air is the major fraction of methane even in dust-rich, glacial ice from
348 Greenland prone to $CH_{4(xs)}$ production (see below). The opposite is expected for ethane and
349 propane, which are dominated by the *in extractu* component in dust-rich Greenland ice. To
350 establish a better knowledge of alkanes in Greenland ice, we evaluated the measured
351 concentrations of methane, ethane, and propane, their ratios to each other and the relation to the
352 content of mineral dust in the ice for both the 1st and the 2nd extraction.

353

354 Note that different units to indicate concentrations of the trace gases of interest are used
355 throughout this study. By using mixing ratios in units of [ppb], as typically used for atmospheric
356 concentrations, the concentration of trace gases is related to the amount of air extracted from
357 the ice. Ice core samples with a low air content cause higher mixing ratio values for any
358 additional molecules produced in situ or *in extractu* compared to ice core samples with a high
359 air content and the interpretation might be biased. Alternatively, for any additional molecules
360 produced in situ or *in extractu*, [mol absolute per sample] denotes the absolute amount of trace
361 gases and is independent of the ice core air content. In the following, both units are used and
362 great care has to be taken to avoid misinterpretation of the results with respect to the different
363 units.

364

365 **3.1.1 Excess alkanes in the 1st extraction**

366

367 Figure 4 and 5 show results from the 1st extraction of our NGRIP and GRIP ice core samples.
368 For dust-rich samples, ethane ranges between 2 ppb and 12 ppb, and propane concentrations
369 between 1 ppb and 5 ppb. In contrast, low-dust samples from both GRIP and NGRIP have much
370 lower concentration (ca. 0.5 ppb for ethane, and 0.3 ppb for propane) consistent with estimates
371 of past atmospheric ethane and propane concentrations from the 15th to 19th century of the
372 common era being about 0.4 ppb in Greenland ice (Nicewonger et al., 2016) and lower for
373 propane (Helmig et al., 2013). Emissions of ethane and propane were likely reduced during the
374 glacial (Bock et al., 2017; Nicewonger et al., 2016; Dyonisius et al., 2020) thus, 0.5 ppb appears
375 to be an upper limit of past atmospheric concentrations of ethane and propane. This estimate of
376 past atmospheric ethane concentrations is an order of magnitude smaller than the values we
377 obtained from our dust-rich ice core samples from the 1st extraction, pointing to a strong

378    additional source of these alkanes for dust-rich samples. Thus, the unusually high mixing ratios

379    indicate that ethane and propane in glacial ice extracted using our melt technique on discrete

380    samples do not represent atmospheric levels.

381

382    As illustrated in Fig. 4 (left panel), the ethane and propane concentrations are highly correlated,

383    pointing to a common production of excess ethane and excess propane. The weighted mean

384    ratio and its weighted standard deviation (both weighted according to the number of samples

385    measured per bag) is (2.25 ± 0.09) ppb ethane/ ppb propane. Note that all regression lines are

386    calculated by following the method of York (1968) and York et al. (2004). York's analytical

387    solution to the best-fit line accounting for normally distributed errors both in x and y is widely

388    used to determine an isotopic mixing line and has been proven as the least biased method (Wehr

389    and Saleska, 2017; Hoheisel et al., 2019). Throughout the manuscript we use the 1 sigma (1 $\sigma$)

390    standard deviation to express uncertainties. In Fig. 4, where the individual bags studied are

391    color-coded, we can clearly see that the ratio is essentially the same between the individual bags

392    and that the correlation is also very high within each bag (although we have to consider for the

393    significance of this correlation that the number of samples per bag is very low). This indicates

394    that for NGRIP ice ethane and propane are found in a fixed ratio. Accordingly, excess ethane

395    and propane production can be well represented by the weighted mean ratio and ethane and

396    propane are produced in a ratio of approximately 2:1. Very similar results were also observed

397    in NGRIP samples measured in 2011 and in GRIP samples revealing an ethane to propane ratio

398    of 2.14 ± 0.03 ($r^2$ = 0.99) and 2.00 ± 0.13 ($r^2$ = 0.99), respectively (see Fig. 4, left panel).

399
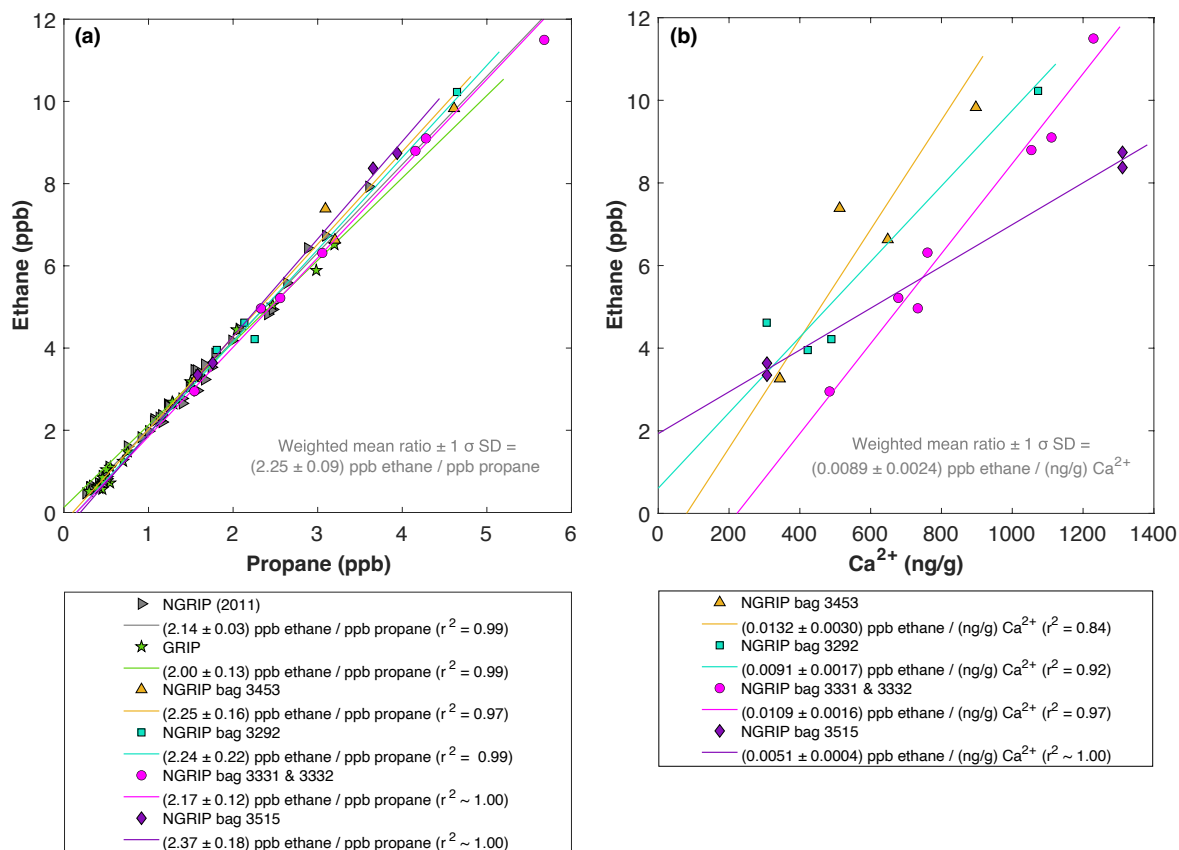
*Figure 4:* **NGRIP and GRIP results of ethane and propane from the 1ˢᵗ extraction. (a)** Concentrations of ethane and propane and their ratios to each other for NGRIP and GRIP samples measured in the 1ˢᵗ extraction of the $\delta^{13}$C-CH$_4$ device. Colors and symbols indicate the different NGRIP bags or cores used. **(b)** Bag-specific production ratios of ethane in relation to the Ca$^{2+}$ concentration for NGRIP samples. Note that for bag 3515 there is a data gap in the Ca$^{2+}$ record and an anomaly of the Ca$^{2+}$ to dust mass ratio for the replicate sample at 1932.7 m. Thus, the Ca$^{2+}$ concentration for these two data points is likely overestimated (see Fig. A3).

Methane concentrations range from 407 ppb to 476 ppb and are predominantly of atmospheric origin (see Fig. 5). The amount of CH$_{4(xs)}$ is the difference between the measured methane concentration and the atmospheric background concentration. To quantify CH$_{4(xs)}$ we use the fact that due to the low-pass filtering of the bubble enclosure process all samples within one bag should have the same atmospheric CH$_4$ concentration. This also ensures that any physical processes that potentially influence the atmospheric alkanes in our samples (gravitational enrichment, thermodiffusion, disequilibrium effects on CH$_4$ isotopes) are the same for all samples within one bag. The only difference between these samples is, thus, the degree of CH$_{4(xs)}$ production which can be estimated from the linear fit between the measured CH$_4$ concentration and the concentration of another species (e.g. ethane, propane, mineral dust, or Ca$^{2+}$), which serves as a proxy for CH$_{4(xs)}$ production. The closest relationship was found for [C$_2$H$_6$] and quantifying CH$_{4(xs)}$ was done by extrapolating the linear regression between ethane

420   and methane to an ethane concentration of 0.39 ppb, the assumed atmospheric [$C_2H_6$]. This

421   leads to an estimate of the true atmospheric [$CH_4$] value within the respective bag, a value that

422   can then be subtracted from the measured $CH_4$ concentration to obtain the $CH_{4(xs)}$ in each

423   sample. The uncertainty of the calculated $CH_{4(xs)}$ is typically 8 ppb.

424

425   Using the relation of ethane to methane this approach translates into $CH_{4(xs)}$ in the range of 14

426   ppb to 91 ppb for these five NGRIP bags with a mean excess of 39 ppb. Equivalent calculations

427   can be made using propane, dust, or $Ca^{2+}$ as proxy for $CH_{4(xs)}$ production, however, the

428   relationship between dust parameters and $CH_{4(xs)}$ is more variable and does not lead to equally

429   precise values for $CH_{4(xs)}$. Nevertheless, the obtained mean $CH_{4(xs)}$ using the relation of mineral

430   dust or $Ca^{2+}$ to methane is similar in size to the one obtained by ethane.

431

432   We find a constant production ratio between all three excess alkanes for all bags investigated.

433   The weighted mean production ratio and its weighted standard deviation was calculated to be

434   (6.42 ± 1.57) ppb methane / ppb ethane and (14.3 ± 3.7) ppb methane/ ppb propane for the

435   samples of the five main NGRIP bags, and (2.25 ± 0.09) ppb ethane/ ppb propane (also

436   including NGRIP2011 and GRIP here). Note that there is a flagged sample for $CH_4$ in bag 3453

437   (yellow asterisk in Fig. 5), where one vent (V6) was unintentionally open during the

438   measurement, which may have compromised the result. We therefore excluded the production

439   ratio determined from bag 3453.

440

441   In summary, we can characterize the excess alkane production in our measured NGRIP samples

442   by an overall methane/ethane/propane ratio of approximately 14:2:1. This constant relationship

443   between different alkanes suggests that excess alkanes are produced in a fixed ratio by a

444   common production process.

445

446   Another important observation is the close relation between excess alkanes and the content of

447   mineral dust within the ice core samples. Using measurements on GISP2 and NEEM ice core

448   samples, Lee et al. (2020) reported for the first time the close relation of $CH_{4(xs)}$ to chemical

449   impurities with the highest correlation with $Ca^{2+}$. This is supported by our measurements on

450   NGRIP and GRIP samples revealing an overall increase of $CH_{4(xs)}$, ethane, and propane with

451   increasing $Ca^{2+}$ (see for example the ethane/$Ca^{2+}$ relationship in Fig. 4, right panel). Although

452   the connection between ethane and $Ca^{2+}$ is more variable than for ethane and propane between

453   the different bags, the slopes of the linear regressions in Fig. 4 (right panel) are still the same

454 within the 2 σ uncertainty and the weighted mean ratio of all NGRIP samples amounts to
455 $(0.0089 \pm 0.0024)$ ppb ethane/ (ng/g) $Ca^{2+}$. However, this weighted mean value is likely biased
456 low due to the relatively low ethane/ $Ca^{2+}$ slope of bag 3515. Due to a data gap at 1932.7 m in
457 the $Ca^{2+}$ record, the corresponding $Ca^{2+}$ concentration for two of the samples of this bag is
458 subject to a large interpolation error and overestimated $Ca^{2+}$ (see Fig. A3).
459

460 The results agree with results from GRIP and earlier NGRIP (2011) measurements, revealing
461 an ethane/ $Ca^{2+}$ ratio of $0.0105 \pm 0.0029$ ($r^2 = 0.76$) and $0.0090 \pm 0.0006$ ($r^2 = 0.91$),
462 respectively.
463 Based on the fixed ratio of $CH_{4(xs)}$ and ethane described above this translates into a weighted
464 mean excess $CH_4/Ca^{2+}$ ratio of $(0.0529 \pm 0.0111)$ ppb methane per (ng/g) $Ca^{2+}$.
465
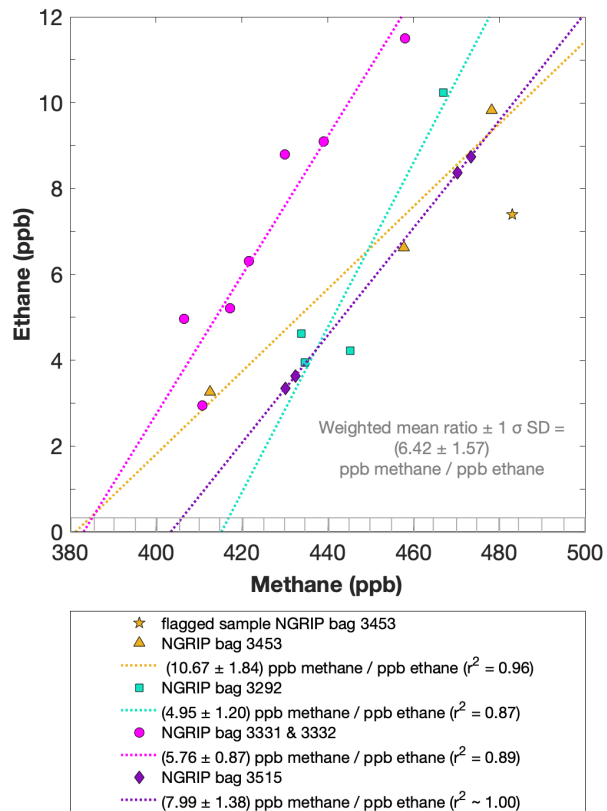
466

467 *Figure 5: **NGRIP** results of methane and ethane from the 1<sup>st</sup> extraction*. Concentrations of methane (ppb) and
468 ethane (ppb) and their ratios to each other for NGRIP samples measured in the 1<sup>st</sup> extraction of the $\delta^{13}C$-$CH_4$
469 device. Different colors and symbols indicate the different NGRIP bags used for our analysis. Note that there is a
470 flagged sample for $CH_4$ in bag 3453 as indicated with a yellow asterisk, which is not included in the ratio of bag
471 3453. The grey hatched area indicates past atmospheric ethane concentrations of maximum 0.39 ppb as estimated
472 by Nicewonger et al. (2016).

473

474

475

### 3.1.2 Excess alkanes in the 2nd extraction

With the 2nd extraction of the $\delta^{13}$C-CH$_4$ analyses we can evaluate the temporal dynamics of excess alkane production, assuming that all alkanes extracted in the 2nd extraction were produced after the 1st extraction was completed.

For our Greenland samples we measured a range of about 0.2 to 2.4 pmol for ethane and a range of 0.1 to 1.2 pmol for propane in the 2nd extraction (Fig. 6, right panel). These values in pmol are equivalent to 0.2 to 4.8 ppb of ethane and 0.2 to 2 ppb of propane assuming that the amount of excess alkanes was added to 14 mL of ice core air (which is the typical ice sample size of 150 g with a total air content of 0.09 mL/g). The measured amount of methane ranges between 3 pmol and 20 pmol (Fig. 6, left panel).

The ratio of the measured amount for the individual species between the 1st and the 2nd extraction amounts to 3.6 ± 0.85 ($r^2$ = 0.78) for ethane (Fig. 7, right panel), 3.3 ± 0.33 ($r^2$ = 0.78) for propane (combined data of NGRIP and GRIP) and 3.8 ± 1.62 ($r^2$ = 0.33) for methane (only NGRIP data), where the uncertainty for CH$_4$ is again much larger. Thus, we can conclude that the amount of alkanes produced during the waiting time after the 1st extraction until the 2nd extraction was finished, was approximately 30% of the amount produced during the 1st extraction. Results from the 2nd extraction also demonstrate that this process is slow and not completed during the 1st extraction. We can thereby confirm the results of Lee et al. (2020) but we are able to show for the first time that this process leads also to production of excess ethane and propane.

For a better estimate of the temporal reaction kinetics of the underlying process, we can relate the measured amount of the individual species to the time available for a potential reaction in the meltwater during each extraction. For the five GRIP samples that were measured with a 2nd and 3rd extraction (see Sec. 2.2 for details) we take the cumulative production amount (where the first data point is the produced amount in the 1st extraction, the second data point is the sum of the 1st and 2nd extraction, and the third data point is the sum of the 1st, 2nd, and 3rd extraction). In the example shown for ethane (Fig. C1, Appendix C), we can see the assumed first-order reaction kinetics with a decreasing ethane accumulation over time providing a good model for our measurements (details on the calculation can be found in Appendix C). With that, we can estimate the half-life time ($\tau$) of the production to be approximately 30 min. Note that this long half life has also an implication for a potential excess production of CH$_4$ in continuous flow

510 techniques, where the time before the air is separated from the liquid water stream is only 1-2
511 min. Thus, only 5-10 % of the *in extractu* production found in our 1st extraction can be expected
512 in such continuous flow techniques, which are difficult to detect.

513

514 The goodness of fit of the ratios of the measured concentrations between the 1st and the 2nd
515 extraction is $r^2 = 0.78$ for both ethane and propane, indicating that the production/release in the
516 1st extraction in relation to the 2nd extraction is well correlated for both species (see Fig. 7b for
517 ethane). Thus, samples that produced higher excess alkanes during the 1st extraction also
518 produced more excess alkanes in the 2nd extraction, suggesting that the production is dependent
519 on the amount of some reactant present in the samples from which excess alkanes are produced.
520 Again, for $CH_4$ this relationship is more variable which is likely related to the higher uncertainty
521 in measuring $CH_4$ for the 2nd extraction.

522

523 The ratio of ethane to propane of all measured Greenland samples in the 2nd extraction is 1.98
524 $\pm$ 0.07 ( $r^2 = 0.99$). The ratio of methane to ethane is 8.17 $\pm$ 1.14 ($r^2 = 0.86$). Accordingly, the
525 overall relationship between methane, ethane, and propane in the 2nd extraction can be
526 characterized by a ratio of approximately 16:2:1. However, comparing the ratios of
527 ethane/propane and methane/ethane between the 1st and the 2nd extraction, there is no significant
528 difference within the 2 $\sigma$ uncertainties from 2.25 $\pm$ 0.09 to 1.98 $\pm$ 0.07, and from 6.42 $\pm$ 1.57 to
529 8.17 $\pm$ 1.14. We can conclude that within the error limits, the production ratios stayed the same,
530 suggesting that the same *in extractu* process is at play during both extractions.

531

532 In the 2nd extraction, we can again observe the relation between excess alkanes and the amount
533 of mineral dust. Figure 7a shows the correlation of ethane (fmol/g meltwater) to $Ca^{2+}$ (ng/g) in
534 all measured NGRIP and GRIP samples in the 2nd extraction revealing a production of (0.0085
535 $\pm$ 0.0011) fmol/(g meltwater) ethane per (ng/g) $Ca^{2+}$ with $r^2 = 0.70$. For methane, we observe a
536 production ratio of (0.0556 $\pm$ 0.01513) fmol/(g meltwater) methane per (ng/g) $Ca^{2+}$ with a
537 correlation of $r^2 = 0.47$ (data not shown).

538

539 Overall, excess alkane concentrations increase with increasing $Ca^{2+}$ concentrations, in both the
540 1st and the 2nd extraction. The total alkane production/release, however, decreased in the 2nd
541 extraction, suggesting the progressive exhaustion over time of some reactant necessary for the
542 *in extractu* process. We propose that this reactant co-varies with $Ca^{2+}$ and particulate dust,

543 where Ca$^{2+}$ is of course not a reactant itself and represents only a proxy for higher *in extractu*

544 production.

545
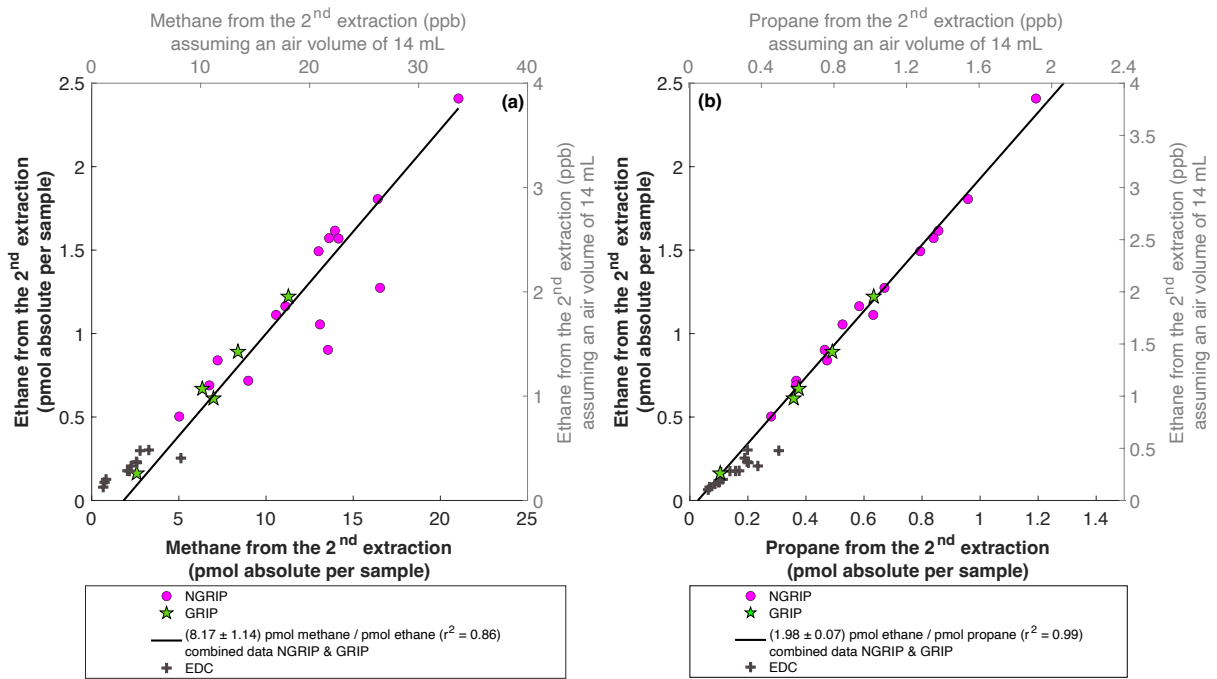
546

547 *Figure 6:* **NGRIP and GRIP results of excess methane, ethane, and propane from the 2$^{nd}$ extraction. (a)**
548 Concentrations of methane and ethane and their ratios to each other. **(b)** Concentrations of propane and ethane and
549 their ratios to each other. Units are given as pmol absolute per sample on the primary axis in black and in ppb
550 assuming an air volume of 14 mL of the ice core sample on the secondary axis in grey. Crosses indicate the blank
551 level of the system estimated from 2$^{nd}$ extractions of EDC ice core samples.

552
553
554
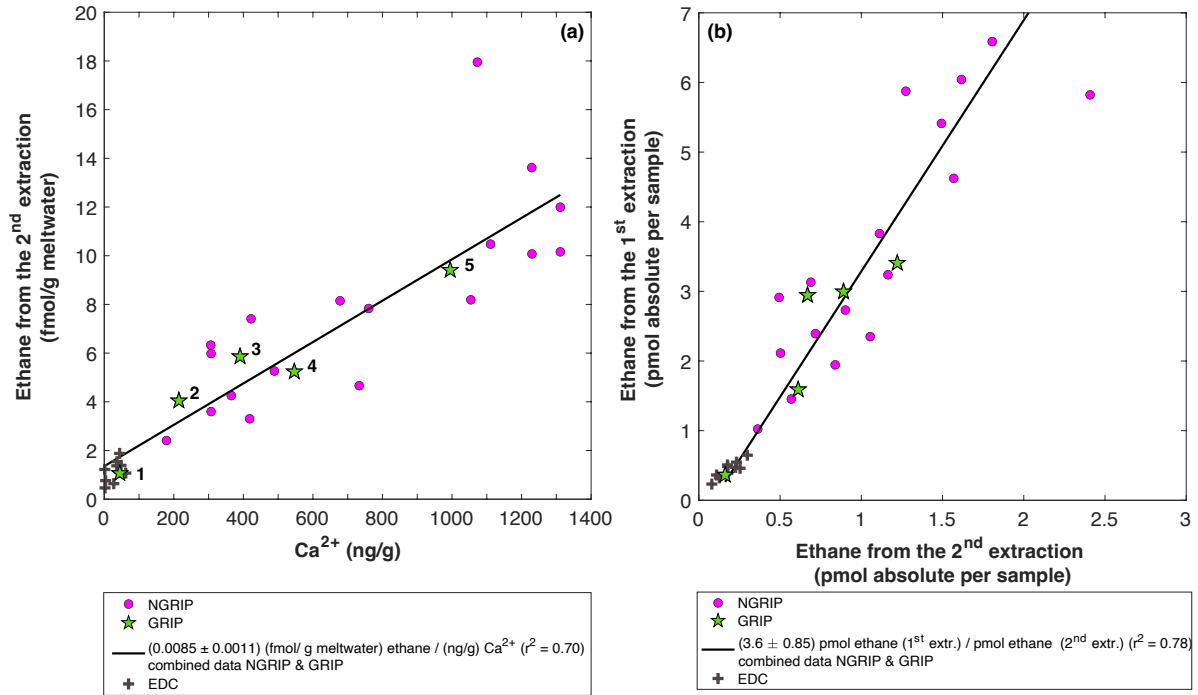
557  Figure 7: **GRIP and GRIP results of ethane from the 2nd extraction in relation to the Ca²⁺ concentration**
558  **and to the 1st extraction. (a)** Produced amount of ethane in the meltwater (fmol/g meltwater) in relation to the
559  $Ca^{2+}$ concentration in the ice core samples. The numbered GRIP samples are used in Figure C1 to evaluate the
560  temporal dynamics. Crosses indicate the blank level of the system estimated from 2nd extractions of EDC ice
561  core samples. **(b)** Relation of the amount of ethane (pmol) measured in the 1st and 2nd extraction.

562
## 563  3.2 Isotopic composition of excess methane
564

565  In this section we characterize the isotopic signature of excess methane and explore how we

566  can use this parameter to better identify its source or production pathway. The evaluation of the

567  carbon and deuterium isotopic signature of excess methane ($\delta^{13}C\text{-}CH_{4(xs)}$ and $\delta D\text{-}CH_{4(xs)}$) is

568  based on the Keeling-plot approach (Keeling, 1958, 1961; Köhler et al., 2006).

569
### 570  3.2.1 $\delta^{13}C\text{-}CH_4$ isotopic signature of excess methane
571

572  Figure 8 (left panel) shows the $\delta^{13}C\text{-}CH_4$ results of the 1st extraction. The carbon isotopic

573  signature of excess $CH_4$ from the 1st extraction of the ice core sample measurements within one

574  NGRIP bag are obtained from the y-intercept of the Keeling-plot, representing the excess $\delta^{13}C\text{-}$

575  $CH_4$ value for this bag. Note that the two NGRIP bags 3331 and 3332 are neighbouring bags

576  and were therefore combined into one Keeling y-intercept. As the individual samples in these

577  two bags span less than 10 years between each other, they are the same within the age

578  distribution, and the assumptions for the Keeling-plot approach (see Sec. 2.1) are met. All bags

579  show agreement in $\delta^{13}C\text{-}CH_4$ signature (y-intercepts) within 2 σ uncertainties. The weighted

580   mean isotopic signature is (-47.0 ± 2.9) ‰, with weights assigned by the number of samples

581   that constrained each individual Keeling plot regression line.

582   With the small number of samples that go into the determination of the y-intercept and its error

583   in the Keeling plot for each individual bag, the estimates of the y-intercepts and their error have

584   to be regarded statistically uncertain. However, comparing the results for the individual bags,

585   they all agree within each within the estimated errors. In order to get a more representative

586   value for the isotopic signature of excess CH4 and its error, we calculate a weighted average

587   for all bags for the y-intercept and its error. Nevertheless, this weighted error may still not be

588   entirely representative because of the small sample number and the true error may likely be

589   somewhat higher.

590

591   Figure 8 (right panel) shows the isotopic results in relation to the amount of CH4 produced

592   during the 2nd extraction. No atmospheric CH4 is present during the 2nd extraction and the

593   individual isotopic values in Fig. 8 (right panel) are the directly measured values of excess CH4

594   without applying the Keeling-plot approach. For a better comparison, the produced CH4 is

595   shown both in pmol (lower axis in Fig. 8, right panel) and in a mixing ratio CH4 scale (ppb).

596   The Keeling y-intercept values of the 1st extraction are added in the right panel of Fig. 8.

597

598   The $\delta^{13}$C-CH4 values of the 2nd extraction range between -34 ‰ and -48 ‰ with the mean being

599   (-41.2 ± 2.2) ‰. This value appears isotopically somewhat heavier compared to the weighted

600   mean of (-47.0 ± 2.9) ‰ inferred from the Keeling analysis, however, is still the same within

601   the 2 σ error limits. We note that the measured peak areas for the 2nd extractions are very small

602   and lie outside of the typical range of our gas chromatography mass spectrometry analysis for

603   $\delta^{13}$C-CH4 and we cannot exclude some bias in these results. However, we mimicked these small

604   peak areas with injections of small amounts of standard air and observed no significant bias in

605   the measured $\delta^{13}$C-CH4 values given that the precision of such small peaks is around 2 ‰.

606

607   Another caveat is the considerable blank contribution for CH4 that we observe for the 2nd

608   extraction. Since Antarctic ice cores do not show a sizable *in extractu* production (Fig. 7,

609   crosses for EDC) we measured EDC samples with the same protocol of a 2nd extraction as for

610   our Greenland samples to provide an upper boundary of this blank. Hence the 2nd extraction of

611   the EDC samples are a conservative blank estimate while the true system blank is lower. As

612   can be seen in Fig. 8 (right panel) the amount of CH4 measured for these EDC samples (crosses)

613   is on average about 2 pmol (equivalent to about 3 ppb). For comparison, our ice samples from

614 Greenland show a range of about 5 to 20 pmol, indicating a considerable blank contribution in

615 the 2nd extraction.

616

617 To estimate the influence of the blank on the isotopic signature that occurs during the 2nd

618 extraction we used the values from our EDC measurements and applied an isotope mass balance

619 approach. The $\delta^{13}$C-CH$_4$ blank signature obtained from these EDC samples is -39.0 ‰, hence

620 a few ‰ heavier than the mean $\delta^{13}$C-CH$_4$ signature of the excess CH$_4$ from this 2nd extraction

621 for the Greenland samples. On average, the correction would shift our NGRIP values towards

622 lighter (more negative) values by 0.31 ‰. This systematic correction is thus small compared to

623 the typical measurement precision obtained both from the Keeling-plot approach and the direct

624 measurement of the CH$_{4(xs)}$ with the 2nd extraction. As the $\delta^{13}$C-CH$_4$ signature of the blank is

625 close to the NGRIP values, performing a blank correction has only little leverage. Considering

626 these analytical limitations of our 2nd extraction for $\delta^{13}$C-CH$_4$, these findings suggest that

627 CH$_{4(xs)}$ produced during the 1st and 2nd extraction has the same $\delta^{13}$C-CH$_4$ isotopic signature

628 within the 2 σ error limits and is likely produced/released by the same process in both

629 extractions.

630
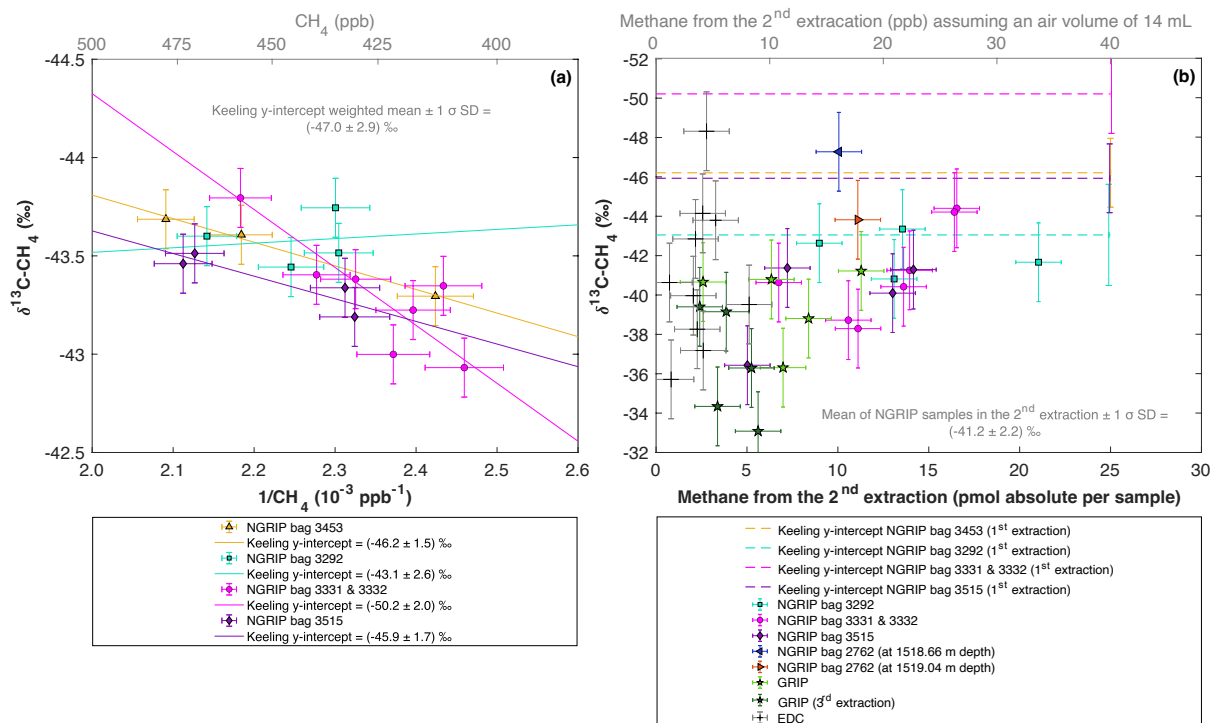
631

632 *Figure 8:* **NGRIP (and GRIP) $\delta^{13}$C-CH$_4$ results of the 1st and 2nd extraction measured with the $\delta^{13}$C-CH$_4$**
633 **device. (a)** Keeling-plot of $\delta^{13}$C-CH$_4$ for NGRIP samples from the five main bags (3292, 3331 & 3332, 3453,
634 3515) measured in the 1st extraction. Colors and symbols indicate individual measurements of the respective bags.
635 Colored lines indicate the corresponding Keeling regression line of each individual bag. **(b)** $\delta^{13}$C-CH$_4$ (‰) values
636 in relation to the amount of methane measured for the 2nd extraction. Units for CH$_4$ are given as pmol absolute per
637 sample on the primary axis in black, and in ppb assuming an air volume of 14mL of an ice core sample on the
638 secondary axis in grey. Colors and symbols indicate individual measurements of the respective bags. Color-coded

639 lines indicate the corresponding Keeling y-intercept of each individual bag as measured in the 1st extraction. Grey
640 crosses indicate the blank level of the system estimated from 2nd extractions of EDC ice core samples.

641

642 **3.2.2 $\delta$D-CH$_4$ isotopic signature of excess methane**

643

644 Figure 9 shows the results of the $\delta$D-CH$_4$ analyses. Due to the larger sample size required for

645 the $\delta$D-CH$_4$ analyses and the sample availability restrictions, only two bags could be measured

646 for $\delta$D-CH$_4$. The individual $\delta$D-CH$_4$ results obtained from the ice core sample measurements

647 within one NGRIP bag are again combined into one Keeling y-intercept, representing the $\delta$D-

648 CH$_4$ value for this bag. NGRIP bag 3460 (orange) reveals a Keeling y-intercept $\delta$D-CH$_4$ value

649 of (-308 ± 51) ‰. The two NGRIP bags 3266 and 3267 (purple) are neighbouring bags and

650 were combined into one Keeling y-intercept revealing a $\delta$D-CH$_4$ value of (-341 ± 62) ‰. The

651 difference between the two Keeling y-intercepts is within the error limits. Accordingly, we

652 combine the two values to a weighted mean and weighted uncertainty of (-326 ± 57) ‰. As

653 stated above, with the small number of samples that go into the determination of the y-intercept

654 and its error in the Keeling plot for each bag, the estimates of the y-intercepts and their error

655 have to be regarded statistically uncertain.

656 Our results are consistent with the findings of Lee et al. (2020), who used the NGRIP $\delta$D-CH$_4$

657 record of Bock et al. (2010b) and the NGRIP [CH$_4$] record of Baumgartner et al. (2014) to

658 estimate the $\delta$D-CH$_{4(xs)}$ signature in these samples. Assuming a two-component mixture of

659 atmospheric methane and excess methane in their model led to a best estimate of (-293 ± 31)

660 ‰ for $\delta$D-CH$_{4(xs)}$ which is within the error limits of our Keeling-plot results.

661
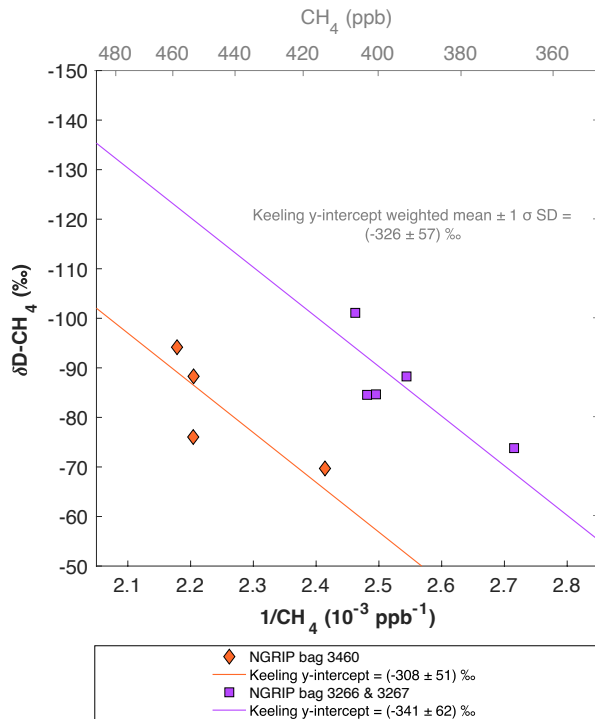
Figure 9: **NGRIP δD-CH₄ results.** Keeling-plot of δD-CH₄ of NGRIP samples measured with the δD-CH₄ device.
Colors and symbols indicate individual measurements of the respective bags and lines indicate the corresponding
regression of each bag.

## 4. Testing the hypotheses explaining excess alkanes

In Sect. 3 several pieces of evidence for the production/release of excess alkanes in Greenland
ice core samples were collected:

- We can confirm the observations of Lee et al. (2020) on excess methane in different
  Greenland ice cores and its covariance with the amount of mineral dust in the ice.
  Despite the different extraction techniques applied (multiple melt-refreeze method in
  Lee et al. (2020) versus two subsequent wet extractions in our study), we can further
  corroborate that the temporal dynamics of the production/release is on the order of hours
  and production/ release occurs when liquid water is present during extraction.
- We document for the first time a co-production/release of excess methane, ethane, and
  propane, with the observed values for ethane and propane exceeding by far their
  estimated past atmospheric background concentrations.
- Excess alkanes (methane, ethane, propane) are produced/ released in a fixed molar ratio
  of approximately 14:2:1, indicating a common origin.

683      -      We further characterize the isotopic composition of excess $CH_4$ of $\delta^{13}C$-$CH_{4(xs)}$ and $\delta D$-

684          $CH_{4(xs)}$ to be (-47.0 ± 2.9) ‰ and (-326 ± 57) ‰ in NGRIP ice core samples,

685          respectively. Within the error limits, our $\delta D$-$CH_{4(xs)}$ results are consistent with the

686          calculated best estimate of (-293 ± 31) ‰ by Lee et al. (2020).

687

688 In the introduction we presented the hypotheses proposed by Lee et al. (2020) explaining their

689 observations on $CH_{4(xs)}$. Here we resume the discussion of the original hypotheses and refine

690 them in light of our new data from NGRIP and GRIP measurements. An overview of the

691 possible sources explaining excess alkanes is illustrated in Fig. 10 and Table 1. We discuss in

692 the following three options for the origin of the observed excess alkanes:

693

694 1.) Excess alkanes could be adsorbed on mineral dust particles prior to their deposition on the

695 Greenland ice sheet and released in the laboratory during the prolonged melting process. The

696 adsorption step could happen in the mineral dust source region (East Asian deserts) thereby

697 adsorbing the alkanes from natural gas seeps within the sediment (process marked as A1, see

698 Fig. 10). Alternatively, adsorption of atmospheric alkanes on dust particles can happen anytime

699 starting from the soil surface in the dust source region, during atmospheric transport to the

700 Greenland ice sheet, or within the firn layer before pores are closed-off (A2). The desorption

701 of the adsorbed alkanes happens during the melting process for both cases.

702

703 2.) Excess alkanes could be produced microbially. The production happens either in the ice (in

704 situ), the alkanes are adsorbed on dust particles in the ice and then slowly released during the

705 melting phase in the laboratory (M1). Alternatively, the microbial production happens in the

706 meltwater during the melting process (*in extractu)* (M2). A microbial in situ production in the

707 ice without an adsorption-desorption process was already deemed unlikely by Lee et al. (2020)

708 since it is not compatible with the lack of $CH_{4(xs)}$ in the CFA $CH_4$ concentration records.

709 3.) Excess alkanes are produced abiotically, e.g. by the decomposition of labile organic

710 compounds. This chemical reaction can happen either in the ice (in situ), where excess alkanes

711 are then adsorbed on dust particles and subsequently released during the melting process (C1),

712 or in the meltwater during extraction (*in extractu*) (C2). An abiotic in situ production in the ice

713 without an adsorption-desorption process can also be ruled out with the CFA evidence.

714

715 We now discuss these mechanisms in detail and evaluate the viability of the different

716 hypotheses in light of our new experimental observations.

717

718
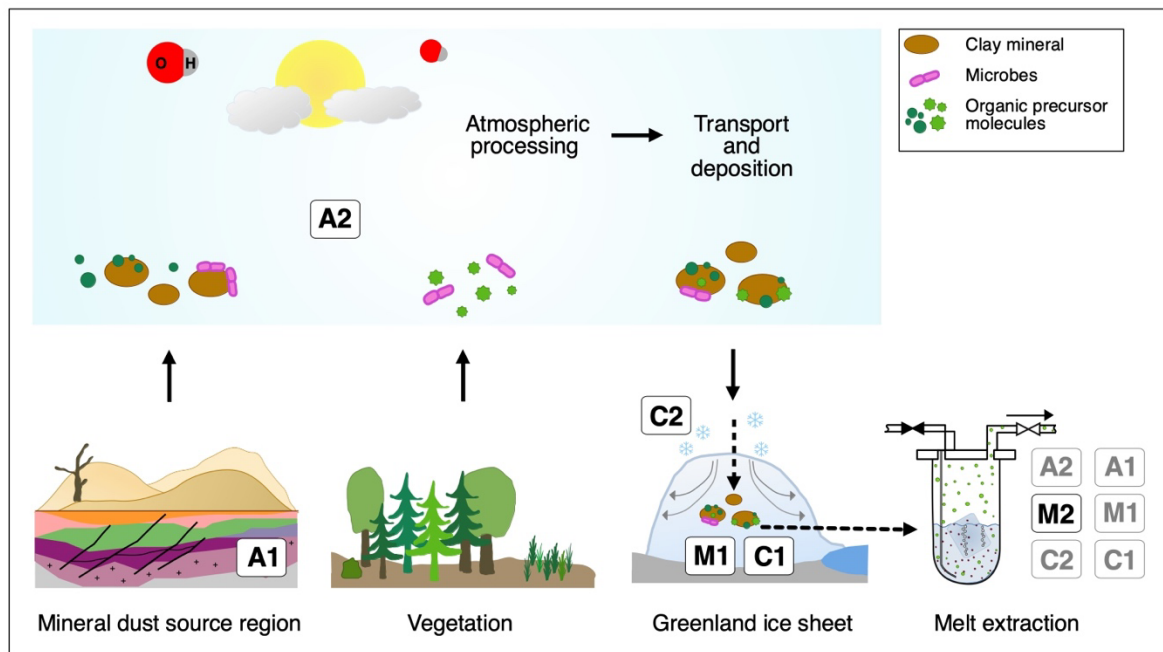
*Figure 10:* **Overview of the different possibilities explaining excess alkanes in dust-rich Greenland ice**. **A** depicts an adsorption process of alkanes on mineral particles, either from natural gas seeps within the sediment (A1) or from the atmosphere (A2) prior to their deposition on the Greenland ice sheet. This gas is then desorbed during melting in the laboratory. **M** depicts a microbial production of excess alkanes, either in the ice (in situ), followed by adsorption on dust particles in the ice and a subsequent slow desorption process during melting (M1), or a microbial production in the meltwater (*in extractu*) (M2). **C** depicts the abiotic/ chemical production of excess alkanes, either in the ice (in situ) followed by adsorption on dust particles after production in the ice and a subsequent slow desorption during the melting process (C1), or an abiotic production in the meltwater (*in extractu*) (C2).

## (1) Adsorption/desorption of alkanes on mineral dust particles

Depending on where the adsorption occurs, the mineral particles might adsorb alkanes of different origin and composition. One possibility is that the adsorption already takes place within the sediment or soil of the dust source region, thus before mineral dust deflation (erosion of loose material by winds from flat and dry areas; A1). As proposed by Lee et al. (2020), the major source region of mineral dust arriving in Greenland during the glacial (Taklamakan, Tarim Basin) are also regions where natural gas seeps reach the surface (Etiope and Klusman, 2002; Etiope et al., 2008). In this case, the measured excess alkanes should reflect the seep's isotopic and alkane composition. Alternatively, adsorption of atmospheric alkanes on the particles can happen anytime starting from the soil surface, during transport en route to the Greenland ice sheet after deflation, and within the firn layer before pores are closed-off (A2). For the scenario A2 the fingerprint (isotopic composition and ratio of alkanes) of the adsorbed alkanes depends on the past atmospheric composition but could be modulated by selective fractionation processes during adsorption and desorption.

744

To be a viable mechanism for our problem, it requires that the adsorbed alkanes stay strongly bound at the dust particles while desorption is minor both during the atmospheric transport and during the several hundred years the dust particles spend in the porous firn (age of the firn at bubble close-off). During the melting procedure the adsorbed alkanes would then be released from their mineral dust carrier, which in case of Greenland ice from glacial times is predominately consisting of clay minerals from the Taklamakan (and partly also Gobi) desert (Biscaye et al., 1997; Svensson et al., 2000; Ruth et al., 2003). However, additional dust sources exist with their relative contribution varying with climate conditions (Han et al., 2018; Lupker et al., 2010).

754

Several experimental studies showed that clay minerals have a high adsorption capacity and retention potential for alkanes (Sugimoto et al., 2003; Cheng and Huang, 2004; Dan et al., 2004; Pires et al., 2008; Ross and Bustin, 2009; Ji et al., 2012; Liu et al., 2013; Tian et al., 2017). Influencing parameters for an adsorption-desorption process are mainly pressure, temperature, clay mineral type, micropore size, surface area, organic carbon content, and water/ moisture content (Sugimoto et al., 2003; Cheng and Huang, 2004; Dan et al., 2004; Pires et al., 2008; Ross and Bustin, 2009; Ji et al., 2012; Liu et al., 2013; Tian et al., 2017). Most interestingly for us, studies by Sugimoto et al. (2003) and Dan et al. (2004) on the adsorption of $CH_4$ in micropores on the surface of clay minerals in dried and fresh lake sediment showed that dried sediment still retains $CH_4$ and that dried and degassed sediment re-adsorbs ambient $CH_4$ at standard pressure and room temperature. The amount of $CH_4$ adsorbed in their samples strongly depends on pressure and temperature while increasing temperatures and decreasing pressure lead to stronger desorption. The addition of water/ moisture leads to a rapid desorption of already adsorbed gases (Sugimoto et al., 2003; Dan et al., 2004; Pires et al., 2008; Ji et al., 2012; Liu et al., 2013).

770

These observations support the possibility of an adsorption-desorption process for our glacial NGRIP and GRIP ice core samples, where alkanes (from fossil seeps or atmosphere) would be adsorbed on dust particles and desorbed during the extraction when liquid water is present. Independent of the origin of the alkanes (A1 or A2), the amount of alkanes adsorbed on dust deposited onto the Greenland ice sheet by this process would be diminished if the dust particles were already in contact with liquid water during the long-range transport which may lead to a loss of previously adsorbed alkanes. This water contact could occur, for example, already at the

778    dust source, as it is known that the deserts in the Tarim basin receive regular input from water

779    from the surrounding mountain regions that also provide the minerals to the basin that are blown

780    out of the desert afterwards (Ruth et al., 2007).

781

782    To explain the constant ratio of methane, ethane, and propane of 14:2:1 in our samples with an

783    adsorption mechanism, we need to discuss the potential origins of the adsorbed alkanes. First,

784    we find very high relative excess contributions of ethane and propane in our samples, while we

785    see a small excess contribution for methane compared to the atmospheric background. This is

786    not in line with the past atmospheric $CH_4/(C_2H_6+C_3H_8)$ ratio where past atmospheric ethane

787    concentrations by Nicewonger et al. (2016) are an order of magnitude smaller (and propane

788    concentrations even less) than the measured concentrations in dust-rich Greenlandice core

789    samples.

790    In contrast, the ratio of methane, ethane, and propane for our samples of approximately 14:2:1,

791    translates into a $CH_4/(C_2H_6+C_3H_8)$ ratio of ~5, which is most consistent with a thermogenic

792    origin (see Fig. 11, left panel). However, due to the different adsorption capacity of mineral

793    dust particles, also a fractionation of the three alkanes is to be expected during the adsorption

794    process, which could alter the thermogenic signature.

795

796    To further evaluate the adsorption theory in light of our experimental results, we now include

797    the carbon and deuterium isotopic signature of $CH_{4(xs)}$ in our samples. Our NGRIP samples

798    reveal a $\delta^{13}C$-$CH_{4(xs)}$ value (Keeling y-intercept weighted mean) of (-47.0 ± 2.9) ‰ which is

799    within the error consistent with contemporaneous atmospheric values or with emissions from

800    seeping reservoirs of natural gas. In contrast, our $\delta D$-$CH_{4(xs)}$ measurements on NGRIP samples

801    reveal a very light  value (Keeling y-intercept weighted mean) of (-326 ± 57) ‰ and slightly

802    outside of the field of a thermogenic origin (see Fig. 11). The value is similar to the estimate

803    by Lee et al. (2020), which, however, lies inside the field of a thermogenic origin (see Fig. 11).

804    While both the low $CH_4/(C_2H_6+C_3H_8)$ ratio and the $\delta^{13}C$-$CH_{4(xs)}$ could be indicative of a

805    thermogenic source (A1), the light $\delta D$-$CH_{4(xs)}$ signature is far away from the atmospheric $\delta D$-

806    $CH_4$ value and is borderline in line with typical $\delta D$-$CH_4$ values of a thermogenic origin. Hence,

807    our $\delta D$-$CH_{4(xs)}$ values exclude the atmospheric adsorption scenario A2 and put a question mark

808    after the seep adsorption scenario A1.

809

810    For the seep adsorption scenario A1 to work the dust particles on which the thermogenic gas

811    adsorbed are not allowed to experience any contact with liquid water prior to the analysis in the

812  lab. In other words, if the particles get in contact with liquid water after the adsorption step, the

813  adsorbed alkanes would desorb from the particles as they do in the laboratory during melting.

814  Given the occurrence of wet/dry cycles in the source area (Ruth et al., 2007), we question the

815  plausibility of scenario A1. Moreover, we expect the characteristic desorption time to differ

816  between the three alkanes, which would be in contradiction to the observation that the alkane

817  ratios in the 1st and 2nd extraction are the same within the error limits.
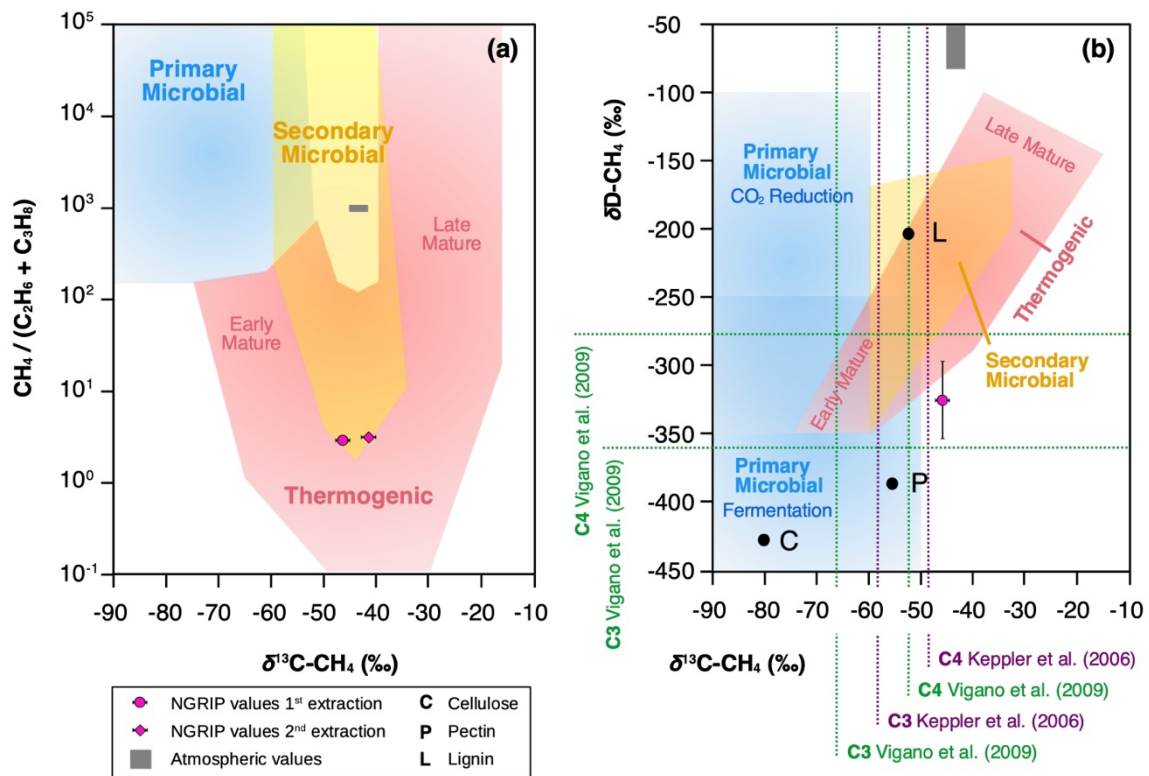
818

819  *Figure 11:* **Diagrams of genetic fields for natural gas adopted from Milkov and Etiope (2018). (a)** Genetic
820  diagram of $\delta^{13}C$-$CH_4$ versus $CH_4/(C_2H_6+C_3H_8)$. Typical atmospheric values are indicated by a grey-shaded area,
821  NGRIP values obtained from the 1st and 2nd extraction from this study with a pink dot. **(b)** Methane genetic diagram
822  of $\delta^{13}C$-$CH_4$ versus $\delta D$-$CH_4$. Values for cellulose (C), lignin (L) and pectin (P) from Vigano et al. (2009) and mean
823  values for C3 and C4 plants, respectively, from studies by Keppler et al. (2006) and Vigano et al. (2009) are added.

824

825

826

827

### (2) Microbial production

829  The second process that we take into consideration is the microbial production of excess alkanes

830  through methanogenic microbes. Here we must again differentiate between two scenarios:

831  microbial production can either take place in the ice sheet  (in situ) by extremophile microbes.

832  This process requires that in situ produced excess alkanes are then adsorbed onto dust particles

833   in the ice and subsequently slowly desorbed during melting when in contact with liquid water
834   (M1). Or the production takes place during the melt extraction when methanogens can
835   metabolize in liquid water (*in extractu*; M2). Lee et al. (2020) already excluded a "simple" in
836   situ production of excess $CH_4$ (microbial in situ production in the ice without an adsorption-
837   desorption process; M0) and this option will therefore not be further discussed here.

838   Our ratios of excess methane/ethane/propane in NGRIP and GRIP samples add another piece
839   of corroborating evidence that excess alkanes are not produced microbially. The main microbial
840   production process of methane, the decomposition of organic precursors in an anaerobic
841   environment by archaea, also co-produces ethane and propane, however only in marginal
842   amounts. The typical methanogenesis yields >200 times more methane than ethane and propane
843   (Bernard et al., 1977; Milkov and Etiope, 2018) while we find a molar ratio of methane to
844   ethane to propane of 14:2:1 in our samples. This renders a microbial production pathway (in
845   situ and *in extractu,* i.e. M1 and M2) unlikely. Moreover, a microbial production of $CH_4$ is
846   unlikely in view of the $\delta^{13}C$-$CH_{4(xs)}$ signature which is too heavy for microbial $CH_4$.

847

848   Apart from these quantitative limitations of microbial $CH_4$ in situ production in ice, there is
849   evidence from the "microbial inhibition experiment" by Lee et al. (2020) against microbial
850   production of alkanes during the melt extraction. Lee et al. (2020) tested whether biological
851   $CH_{4(xs)}$ production in the meltwater was inhibited when the ice core samples were treated with
852   $HgCl_2$. As $CH_{4(xs)}$ was still observed in the poisoned samples and as it seems unlikely that
853   microbes are resistant to $HgCl_2$, this experiment questions the hypothesis of microbially
854   produced $CH_{4(xs)}$ also during extraction (*in extractu*).

855

856   We conclude that regardless of the location of the production, in situ or *in extractu*, the
857   fingerprint of the excess alkanes in our samples (heavy $\delta^{13}C$-$CH_{4(xs)}$ signature and low
858   $CH_4/(C_2H_6+C_3H_8)$ ratio) essentially rules out a microbial source and another (abiotic?) process
859   for excess alkane production is likely to exist.

860

861   **(3) Abiotic/ chemical production**
862   In this last section we consider an abiotic or chemical process to be responsible for the observed
863   excess alkanes, where excess alkanes would be produced through the abiotic decomposition of
864   labile organic compounds in the meltwater (C2). We question an abiotic in situ production in
865   the ice (C1) as it would require the quantitative adsorption of the in situ produced alkanes onto
866   mineral dust particles but not the atmospheric $CH_4$ that is available in the ice otherwise.

867 However, as the location of an in situ excess $CH_4$ production in the ice is not the same as the
868 location of the bubble or clathrates in the ice, this argument is not able to exclude this
869 hypothesis. However, given the age of the ice that allows for permeation of gases on the grain
870 scale and the recrystallization of the ice during that time, which both could bring the
871 atmospheric $CH_4$ in contact with the dust particles, we feel this process is less plausible than a
872 potential C2 mechanism. Moreover (as mentioned before), in view of the expected different
873 desorption characteristics of the three alkanes, we would expect different alkane rations in the
874 1st and 2nd extraction, which is not the case. Accordingly, a direct abiotic production during
875 melting appears to be more likely than a desorption process.

876

877 Organic precursors for this abiotic production during extraction could be any organic matter
878 (either microbial or plant-derived). As the amount of excess alkanes is tightly coupled to the
879 amount of dust, we assume that these organic compounds are attached to dust particles. This
880 "docking" of the organic precursor onto the mineral dust could happen already in the dust
881 source region involving organic material available at the surface. Or it could happen by
882 adhering of volatile organic molecules or secondary organic aerosols from the atmosphere to
883 the mineral dust aerosol either before deflation at the source region or during transport to
884 Greenland.

885

886 We consider this pathway plausible, as in recent years the prevailing paradigm that methane is
887 only produced by methanogenic archaea under strictly anaerobic conditions has been
888 challenged. Several experimental studies demonstrated that methane can also be released from
889 dried soils (Hurkuck et al., 2012; Jugold et al., 2012; Wang et al., 2013; Qian et al., 2016), fresh
890 plant matter and dry leaf litter (Keppler et al., 2006; Vigano et al., 2008, 2009, 2010; Bruhn et
891 al., 2009; Derendorp et al., 2010, 2011), different kinds of living eukaryotes (plants, animals
892 and fungi) (Liu et al., 2015), single organic structural components (McLeod et al., 2008;
893 Messenger et al., 2009; Althoff et al., 2014) and in fact under aerobic conditions. Most of these
894 studies focused on methane, however, there is also evidence for simultaneous formation of other
895 short-chain hydrocarbons like ethane and propane (McLeod et al., 2008; Derendorp et al., 2010,
896 2011). At least three mechanisms have been identified to be relevant: i) photo-degradation, ii)
897 thermal degradation, or iii) degradation by the reaction with a reactive oxygen species (ROS)
898 (Schade et al., 1999; Wang et al., 2017). Common to all three pathways is a functional group
899 (for example a methyl or ethyl group) that is cleaved from the organic precursor molecule. Key
900 parameters that control the production of abiotic methane are mainly temperature, UV radiation,

901  water/ moisture, and the type of organic precursor material (Vigano et al., 2008; Derendorp et
902  al., 2010, 2011; Hurkuck et al., 2012; Jugold et al., 2012; Wang et al., 2013, 2017).

903

904  Recent findings demonstrated the large variety of potential organic precursors for abiotic trace
905  gas formation. For methane formation, the plant structural components pectin and lignin have
906  been identified in many studies as a precursor in different plant materials. Pectin and lignin
907  contain methoxyl-groups in two different chemical types, ester methoxyl (present in pectin) and
908  ether methoxyl (present in lignin) (Keppler et al., 2006, 2008; McLeod et al., 2008; Messenger
909  et al., 2009; Bruhn et al., 2009; Vigano et al., 2008; Hurkuck et al., 2012; Liu et al., 2015; Wang
910  et al., 2017). Ester methyl groups of pectin were also discovered as precursor for ethane
911  formation (McLeod et al., 2008). Overall, pectin makes up a large fraction of the primary cell
912  wall mass of many plants, thus, representing a large reservoir available as precursor for abiotic
913  alkane formation (Keppler et al., 2006; Mohnen et al., 2008; Vigano et al., 2008, 2010; McLeod
914  et al., 2008), and may be present in sufficient quantities in our ice core samples attached to
915  mineral dust particles. $CH_4$ production was also detected from cellulose even though it does not
916  contain methoxyl groups suggesting that other carbon moieties of polysaccharides might allow
917  abiotic $CH_4$ formation (Keppler et al., 2006; Vigano et al., 2008). In addition, poly-unsaturated
918  fatty acids in plant membranes are suggested to play a key role not only in the formation of
919  methane but also for ethane and propane (John and Curtis, 1977; Dumelin and Tappel, 1977;
920  Derendorp et al., 2010, 2011). Further, sulfur-bound methyl groups of methionine are an
921  important precursor for abiotic $CH_4$ formation in fungi (Althoff et al., 2014).

922

923  Considerably different emission rates were found for the same amount but different type of
924  organic substances leading to the conclusion that abiotic emissions are strongly dependent on
925  the type of organic precursor material or single structural components (Keppler et al., 2006;
926  McLeod et al., 2008; Vigano et al., 2008; Messenger et al., 2009; Hurkuck et al., 2012). Other
927  factors such as leaf and cell wall structure (McLeod and Newsham, 2007; Watanabe et al.,
928  2012; Liu et al., 2015) and the organic carbon content (Hurkuck et al., 2012) are suggested to
929  influence this process, too.

930

931  To explain the observed excess alkanes in dust-rich Greenland ice core samples by an abiotic
932  production through the decomposition of labile organic compounds requires adequate quantities
933  of organic precursors within the ice core samples. Certainly, such material is present in
934  Greenland ice, but currently, there is no record on the amount and type of organic substances

available. We have some limited information from occasional Greenland ice core samples in which different types of organic substances were detected (Giorio et al., 2018, and references therein), but it does not allow for an overarching interpretation for our ice samples. A NGRIP record on formaldehyde and a GRIP record on acetate and formate exists (Fuhrer et al., 1997), which suggest lower levels during the glacial, but as we do not know which organic precurors lead to the excess $CH_4$ productions this observation is only of limited value.

We may also question whether a perfect record of eligible precursor molecules could exist at all. As we observe that precursor substances are labile and quickly decompose when in contact with liquid water, a direct measurement of these substances might not be possible but only for similar, non-reactive substances, which are then not qualified as precursors for the reaction observed. The problems of sampling, analysis and interpretation of organic material in polar ice are well summarized and expounded in Giorio et al. (2018).

In any case, it appears likely that the mineral dust carries along soil organic matter or plant residues or accumulates organic aerosols as a result of organic aerosol aging during transport. In our data we see a relationship between the amount of mineral dust within the ice core samples and the amount of excess alkanes. As the amount of excess alkanes per $Ca^{2+}$ (or mass of dust) is variable, this suggests that mineral dust is just a carrier for (a variable amount of) organic substances but does not account for the production of excess alkanes itself. The dust content within the ice core sample can only serve as a rough estimate of organic precursor availability and whether an abiotic production from organic precursor substances is likely to occur during extraction.

Again, our experiments can shed some light on the viability of this pathway for excess alkane production. If we assume that the dust-related organic matter in the ice represents a reservoir available for abiotic production, then the decomposition continues until all functional groups are cleaved from their organic precursor molecules and released as excess alkanes. Once the reservoir is emptied, excess alkane production ceases (Derendorp et al., 2010, 2011). In line, we interpret that the decrease in the amount of measured excess alkanes from the 1st to the 2nd extraction may result from an exhaustion of the precursor reservoir. The reaction time is slow enough to allow for the continuing production during the second extraction but too slow for a detectable production during continuous flow analysis of $CH_4$, where the water phase is present only for less than two minutes before gas extraction. The significantly reduced production

969 during the 2$^{nd}$ extraction in our samples shows that the time scale for this process is hours (see
970 Fig. C1) until the reservoir of functional groups is depleted. We note that this implies that the
971 amount of excess alkanes is strongly dependent on the time span when liquid water is in contact
972 with the dust, which varies among the methods used for $CH_4$ analyses. Thus, any excess $CH_4$
973 in measurements from different labs performed under different conditions may differ.

974

975 To explain an abiotic alkane production, certain conducive boundary conditions must be met.
976 The most important parameters that control non-microbial trace gas formation are temperature
977 and UV radiation. This was demonstrated in many field and laboratory experiments (Keppler
978 et al., 2006; McLeod et al., 2008; Vigano et al., 2008, 2009; Messenger et al., 2009; Bruhn et
979 al., 2009; Derendorp et al., 2010, 2011; Hurkuck et al., 2012; Jugold et al., 2012; Wang et al.,
980 2017). Generally, increasing temperatures lead to exponentially increasing $CH_4$ emissions
981 (Vigano et al., 2008; Bruhn et al., 2009; Wang et al., 2013; Liu et al., 2015). The same behaviour
982 was observed for ethane and propane with very low emissions at ambient temperatures (20-
983 30°C) and a maximum at 70°C (McLeod et al., 2008; Derendorp et al., 2010, 2011). At constant
984 temperatures emission rates decreased over time, which is at high temperatures on the timescale
985 of hours and at ambient temperatures of months. Even after months, some production was
986 observed, pointing to a slowly depleting reservoir of organic precursors (Derendorp et al., 2010,
987 2011). Increasing emissions observed at temperatures >40°C were also used as indicator to
988 exclude the possibility of enzymatic activity, as the denaturation of enzymes would lead to
989 rapidly declining emissions at higher temperatures (Keppler et al., 2006; Derendorp et al., 2011;
990 Liu et al., 2015). We note that our sample extraction takes place at 0°C or a few °C above,
991 hence, temperature conditions during the extraction are not conducive of the type of abiotic
992 alkane production as observed in the studies listed above. Whether the cool temperature of the
993 meltwater during extraction inhibits abiotic reaction is difficult to say. Derendorp et al. (2010,
994 2011) observed a much lower temperature dependency of C2-C5 hydrocarbon emissions from
995 ground leaves than whole leaves, which might also apply to our samples with very fine
996 fragments of organic substances attached to dust particles.

997

998 Besides the strong relationship to temperature also UV irradiation seems to have a substantial
999 effect on abiotic production. Studies on irradiated samples (dry and fresh plant matter, plant
1000 structural components) showed a linear increase in methane emissions, while UV-B irradiation
1001 seems to have a much stronger effect on the release compared to UV-A (Vigano et al., 2008;
1002 McLeod et al., 2008; Bruhn et al., 2009; Jugold et al., 2012). The influence of visible light (400-

1003 700 nm), however, seems controversial (Keppler et al., 2006; Bruhn et al., 2009; Austin et al.,
1004 2016). Further, samples that were heated and irradiated show a different emission curve than
1005 just heated samples, indicating that irradiation changes the temperature dependency, in turn
1006 pointing to the fact that different chemical pathways exist (Vigano et al., 2008).

1007 In dark experiments on plant material at different temperatures $CH_4$ emissions were still
1008 observed, while again higher temperatures revealed much higher emissions, emphasizing the
1009 strong temperature dependency also without UV irradiation (Vigano et al., 2008; Wang et al.,
1010 2008; Bruhn et al., 2009). The release of ethane along with methane from pectin was also
1011 stimulated under UV radiation (McLeod et al., 2008).

1012

1013 Regarding our measurements, the sample vessel in the $\delta^{13}C$-$CH_4$ device is encased by a UV
1014 blocker foil absorbing the shortwave (<600 nm) emissions from the heating bulbs when melting
1015 the ice sample, while in the $\delta D$-$CH_4$ device, the sample vessel is completely shielded from light
1016 (Sect. 2.2 and 2.3). Two NGRIP ice core samples were measured with the $\delta^{13}C$-$CH_4$ device in
1017 the dark ("dark extraction") showing the same amount of excess alkanes as the regular
1018 measurements at day light. This indicates that light >600 nm has no influence on an *in extractu*
1019 reaction during our measurements.

1020

1021 We stress that although we can exclude a direct UV effect during melting, it is possible that UV
1022 irradiation during dust aerosol transport to Greenland and within the upper snow layer after
1023 deposition until the snow gets buried into deeper layers may precondition organic precursors
1024 attached to dust to allow for alkane production to occur during the melt extraction. In particular,
1025 the first step of the reaction (excitation of the homolytic bond of a precursor compound) may
1026 start already in the atmosphere or in the snow where UV radiation is available. Within the ice
1027 sheet the reaction may be paused ("frozen reaction") and the total reaction pathway is only
1028 completed during the melting process when liquid water is present.

1029

1030 Finally, we consider the role of reactive oxygen species in an abiotic production pathway. ROS
1031 are widely produced in metabolic pathways during biological activity but also during
1032 photochemical reactions with mineral oxides (Apel and Hirt, 2004; Messenger et al., 2009;
1033 Georgiou et al., 2015). Through their high oxidative potential, ROS can cleave functional
1034 groups from precursor compounds. Several studies have demonstrated this mechanism for the
1035 production of abiotic $CH_4$ in soils and plant matter (McLeod et al., 2008; Messenger et al.,
1036 2009; Althoff et al., 2010, 2014; Jugold et al., 2012; Wang et al., 2011, 2013) and for other
1037 trace gases such as $CO_2$, ethane, and ethylene from plant pectins (McLeod et al., 2008). UV

1038 radiation or thermal energy has no direct influence on the degradation process by the reaction
1039 with ROS, however, it might also be a stimulating factor and evoke further indirect reactions.
1040 For instance, UV radiation can lead to changes in plants which in turn lead to ROS generation
1041 (Liu et al., 2015). It was demonstrated that UV radiation induces the formation of organic
1042 photosensitizers or photo-catalysts which increase $CH_4$ emissions from pectin (Messenger et
1043 al., 2009) and clay minerals. For example, the formation of hydroxyl radicals from
1044 montmorillonite and other clay minerals upon UV (and visible light) irradiation shows that
1045 clays might play a significant role in the oxidation of organic compounds on their surface
1046 (Katagi, 1990; Wu et al., 2008; Kibanova et al., 2011).

1047

1048 It has been proven that the species type and the overall amount of ROS available for, or involved
1049 in a reaction, has a significant effect on the amount of emissions through such a process (Jugold
1050 et al., 2012; Wang et al., 2013, 2017). For the production of methane (and ethane), hydrogen
1051 peroxide ($H_2O_2$) and hydroxyl radicals have been proven to be the prominent species
1052 (Messenger et al., 2009; Althoff et al., 2010; Wang et al., 2011, 2013; Jugold et al., 2012;
1053 McLeod et al., 2008). Such ROS could be already present in the snow and ice or being produced
1054 in the meltwater. For example, $H_2O_2$ can be unambiguously detected in Greenland Holocene
1055 ice using CFA, however, $H_2O_2$ in dusty glacial ice is mostly below the detection limit, likely
1056 due to oxidation reactions in the ice sheet or during melt extraction.

1057

1058 In summary, we believe that in our case of excess alkane production/ release in the meltwater
1059 at low temperatures and without any UV irradiation, the ROS-induced mechanism appears
1060 possible. In experiments with plant pectin McLeod et al. (2008) observed not only $CH_4$ but also
1061 ethane and found a methane to ethane production ratio of around 5 which is similar to our value
1062 of around 7. Accordingly, we see that a ROS-induced production pathway has the potential to
1063 explain excess alkanes in our samples, however, little is known about ROS chemistry in ice in
1064 particular for reactions with organic precursors and more research is needed to understand the
1065 role of ROS in organic decomposition in ice. Another alternative to the two-stage reaction
1066 pathway with ROS would be a reaction catalyzed in the meltwater by dust-derived transition
1067 metals. This has been observed for example for the oxidation of $SO_2$ in water-activated aerosol
1068 particles (Harris et al., 2013), but to our knowledge it has not been described in the literature
1069 for alkane production via organic precursors so far. Accordingly, we can only speculate on this
1070 pathway at the moment.

1071

1072

1073 Another key parameter influencing all abiotic pathways might be the presence of liquid water

1074 or moisture. In experiments testing the hypothesis of non-microbial $CH_4$ formation in different

1075 soil samples, it was demonstrated that adding water/moisture led to an up to eight-fold increase

1076 in $CH_4$ emissions (Hurkuck et al., 2012; Jugold et al., 2012; Wang et al., 2013). It is

1077 hypothesized that the presence of liquid water or moisture stimulates (in addition to heating or

1078 UV radiation) the cleaving process of a functional group from the primary precursor and

1079 therefore increases the production of $CH_4$. With respect to our observations on NGRIP and

1080 GRIP samples the presence of water seems to be a fundamental parameter influencing the

1081 second step of a "frozen reaction" *in extractu* process, where the duration of water presence

1082 plays an important role.

1083

1084 A final puzzle piece for a possible abiotic methane production comes from our dual isotopic

1085 fingerprints of the excess $CH_4$. As illustrated in Fig. 11 (right panel) our $\delta D$-$CH_{4(xs)}$ signature

1086 lies well within the distribution of the hydrogen isotopic composition of $CH_4$ produced from

1087 potential organic precursors. For $\delta^{13}C$ our values lie outside and on the heavier side of the

1088 carbon isotope signature spectrum.

1089

1090 We conclude that despite our inability to pinpoint the exact organic precursors that lead to

1091 abiotic excess alkane production during the melt extraction of our ice samples, both the ratio of

1092 the excess alkanes as well as the isotopic signature of excess $CH_4$ is generally in line with this

1093 pathway. Thus, without further contradicting evidence from targeted studies on organic

1094 precursors in ice core samples and their chemical degradation, we believe that the ROS-induced

1095 production pathway is to date the most likely explanation for the observed excess alkanes

1096 during extraction. However, we cannot completely rule out an adsorption-desorption process

1097 of thermogenic gas on dust particles.

1098
1099
1100
1101
1102
1103
1104
1105
1106
1107
1108
1109
1110
1111
1112

Table 1: **Overview of the different hypotheses explaining the possible sources for excess alkanes (as illustrated in Figure 10) in relation to our experimental observations.** A green checkmark indicates that the observation is in line with the respective mechanism, a black cross indicates that the observation is in not line with the respective mechanism. A grey shaded area means that this observation does not apply or does not affect the respective mechanism.

| | (1) ADSORPTION-DESORPTION OF THERMOGENIC/ ATMOSPHERIC GAS | | (2) MICROBIAL PRODUCTION | | | (3) ABIOTIC/ CHEMICAL PRODUCTION | |
|---|---|---|---|---|---|---|---|
| | A1 | A2 | M0 | M1 | M2 | C1 | C2 |
| Correlation to $Ca^{2+}$/ mineral dust | ✓ | ✓ | ✓ | ✓ | ✓ | ✓ | ✓ |
| Alkane pattern | ✓ | ✗ | ✗ | ✗ | ✗ | (✓) | (✓) |
| CFA evidence | | | ✗ | | | | |
| $\delta^{13}C$-$CH_{4(xs)}$ | ✗ | ✓ | ✗ | ✗ | ✗ | (✓) | (✓) |
| $\delta D$-$CH_{4(xs)}$ | ✓ | ✗ | ✓ | ✓ | ✓ | (✓) | (✓) |
| $\delta D$-$CH_{4(xs)}$ estimated by Lee et al. (2020) | ✓ | ✗ | ✓ | ✓ | ✓ | (✓) | (✓) |
| Poisoning experiment by Lee et al. (2020) | | | | | ✗ | | |

## 5. Conclusions and Outlook

The comparison of methane records from ice cores samples measured with different melt extraction techniques requires careful consideration and interpretation. Non-atmospheric methane contributions to the total methane concentration were discovered in specific Greenland ice core sections pointing to a process occurring during the wet extraction. To better assess this finding, we measured new records of [methane], [ethane], [propane], $\delta D$-$CH_4$, and $\delta^{13}C$-$CH_4$ on discrete NGRIP and GRIP ice core samples using two different wet extraction systems. With our new data we confirm the production of $CH_{4(xs)}$ in the meltwater and quantify its dual isotopic signature. With the simultaneous detection of ethane and propane we discovered that these short-chain alkanes are co-produced in a fixed molar ratio pointing to a common production pathway. With our 2nd extraction we constrained the temporal dynamics of this process, which occurs on the timescale of hours.

1135 Based on our new experimental data we provide an improved assessment of potential

1136 mechanisms that could explain the observed variations in NGRIP and GRIP ice samples. A

1137 microbial $CH_4$ production represents an obvious candidate, but regardless of whether this $CH_4$

1138 is produced in situ or *in extractu,* several lines of evidence gained from our measurements (low

1139 $CH_4/(C_2H_6+C_3H_8)$ ratio, heavy $\delta^{13}C$-$CH_{4(xs)}$ signature) demonstrate that the fingerprint of the

1140 produced excess alkanes is unlikely of microbial origin. Also an adsorption-desorption process

1141 of atmospheric or thermogenic $CH_4$ on dust particles does not match many of our observations

1142 and is therefore unlikely. However, with the current knowledge we cannot definitely exclude

1143 such an adsorption of thermogenic gas to be responsible for the observed excess alkane levels

1144 in our samples.

1145

1146 At present we favor to explain the formation of excess alkanes by abiotic decomposition of

1147 organic precursors during prolonged wet extraction. Such an abiotic source for methane and

1148 other short-chain alkanes was discovered previously in other studies (Keppler et al., 2006;

1149 Vigano et al., 2008, 2009, 2010; Messenger et al., 2009; Hurkuck et al., 2012; Wang et al.,

1150 2013, and others listed above) using different organic samples, e.g. from plant or soil material,

1151 however, this process has not been connected to excess $CH_4$ production during ice core

1152 analyses. This process matches many of our observations, and such a mechanism can be

1153 responsible for excess alkanes in Greenland ice core samples. To better assess a potential abiotic

1154 production process in ice analyses the most important questions to solve in the future are: What

1155 are the specific precursor substances? Which parameters control an abiotic production during

1156 wet extractions? How does the fixed molar ratio between methane, ethane, and propane come

1157 about in this process? And finally, in which way is this excess alkane production causally

1158 related to the amount of mineral dust within the ice sample?

1159

1160 Identifying a specific reaction pathway that leads to the short-chain alkanes with their observed

1161 ratios would certainly benefit from identifying targeted organic precursor substances in the ice.

1162 However, detecting these postulated organic precursors in the ice core is inherently difficult as

1163 these compounds are very labile in water as our experiments demonstrated that after about 30

1164 min only a fraction of these compounds remains in the meltwater while the majority already

1165 reacted to excess alkanes. Future studies may also focus on further isotope measurements ($\delta^{13}C$-

1166 $CH_4$ and $\delta D$-$CH_4$) including isotope labeling experiments providing an option to

1167 unambiguously detect methane produced during the measurement procedure in a commonly

1168   used wet extraction technique, and again, to uncover potential reaction mechanisms for $CH_{4(xs)}$

1169   production.

1170

1171   To better assess the viability of the alternative hypothesis of a release of previously adsorbed

1172   alkanes from dust particles (scenario A1 and A2) during the extraction, dust particles from the

1173   Taklamakan or Gobi desert need to be tested whether they contain relevant amounts of adsorbed

1174   alkanes that are released when in contact with liquid water. A second step could be to expose

1175   such dust samples to high levels of alkanes to mimic the adsorption process of natural gas seeps.

1176   It also needs to be shown that the adsorbed alkanes stay adsorbed on the dust particles for a

1177   prolonged time (months, ideally years) after exposing the particles to ambient air and that

1178   droplet and ice nucleation during aerosol transport does not lead to a loss of the previously

1179   adsorbed $CH_4$. To quantify any isotopic fractionation involved with the ad- and desorption step,

1180   $\delta^{13}C$-$CH_4$ and $\delta D$-$CH_4$ analyses will be most valuable.

1181

1182   Finally, our studies clearly show that the published Greenland ice core $CH_4$ record is biased

1183   high for selected (glacial, dust-rich) time intervals and needs to be corrected for the excess $CH_4$

1184   contribution. This is particularly important for studies of the IPD in $CH_4$ and stable isotope

1185   ratios of methane. Methodological ways to remedy excess methane (and ethane and propane)

1186   in future measurements of atmospheric $[CH_4]$ from air trapped in ice cores could be to use

1187   continuous online $CH_4$ measurements, which apparently avoid sizeable $CH_{4(xs)}$ production. But

1188   also dry extraction methods and sublimation techniques for discrete samples, which are

1189   expected to avoid *in extractu* production by evading the melting phase, could be used. Finally,

1190   our own $\delta^{13}C$-$CH_4$ device, which allows to measure $\delta^{13}C$-$CH_4$ as well as methane, ethane, and

1191   propane concentrations from the same sample, can be used to correct the measured $CH_4$ values

1192   making use of the co-production of the other two alkanes.

1193

1194   $CH_{4(xs)}$ needs to be corrected for when interpreting the already existing discrete $CH_4$ records

1195   and its stable isotopes in dust-rich intervals in Greenland ice core samples. Impact of $CH_{4(xs)}$ on

1196   interpreting past atmospheric $[CH_4]$ will only slightly affect radiative forcing reconstructions,

1197   however, it will have a significant effect on the assessment of the global $CH_4$ cycle and in

1198   particular on the hemispheric $CH_4$ source distribution which is based on the IPD. We observe

1199   that in some intervals, $CH_{4(xs)}$ is in the same range as the previously reconstructed IPD implying

1200   that correcting for $CH_{4(xs)}$ will lower the IPD considerably and hence lower also the relative

1201   contribution of northern hemispheric sources at those times. We see that there is an urgent need

to reliably revisit Greenland ice core $CH_4$ records for the excess $CH_4$ contribution. In future work we aim to establish an applicable correction for excess methane ($CH_{4(xs)}$, $\delta^{13}C$-$CH_{4(xs)}$, $\delta D$-$CH_{4(xs)}$) in existing records using the co-production ratios of methane, ethane, and propane, the isotope mass balance of excess and atmospheric $CH_4$ in ice core samples as well as the overall correlation of excess $CH_4$ with the mineral dust content in the ice.

**Appendix A**

Figure A1: **Detailed data overview for the neighbouring NGRIP bags 3331 & 3332.** Bag-specific overview of several parameters measured for each sample in this bag: methane, ethane, propane, $Ca^{2+}$, mineral dust mass, TAC (Total Air Content), $\delta^{13}$C-CH$_4$, indicated at the NGRIP depth (bottom axis) and the AICC2012 gas age (upper top axis) and the GICC05 ice age (lower top axis). The mineral dust record is taken from Ruth et al. (2003), the $Ca^{2+}$ record from Erhardt et al. (2022).
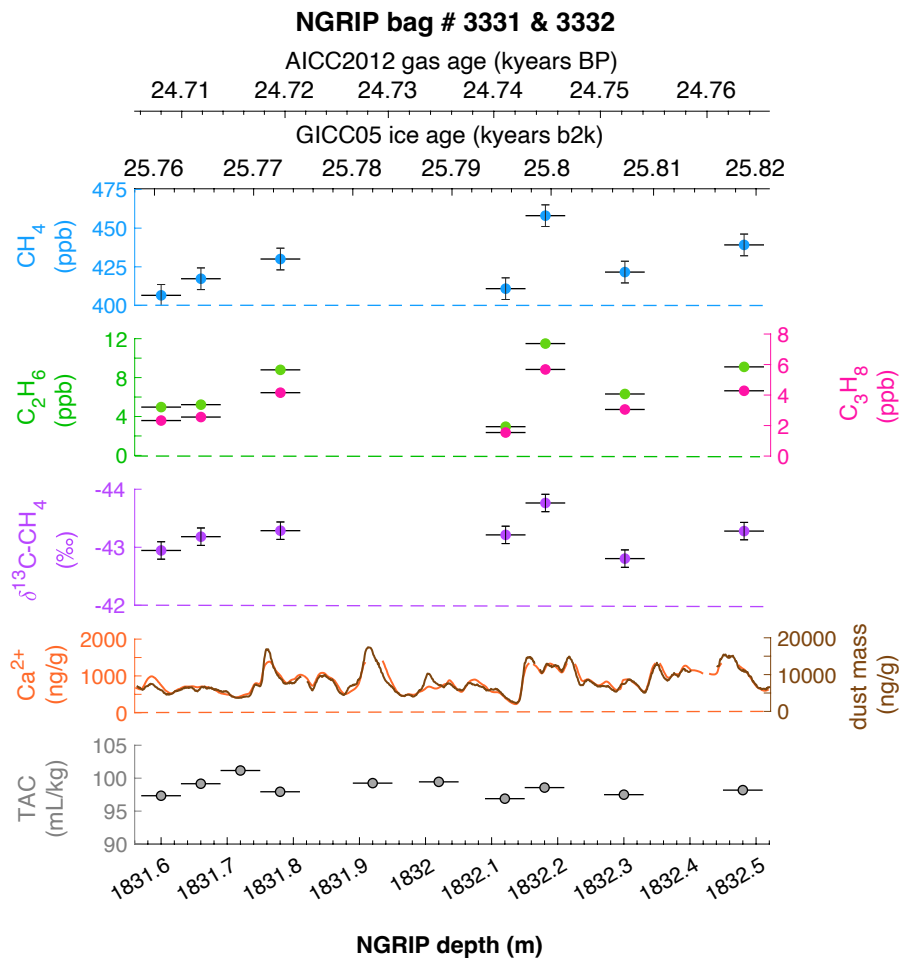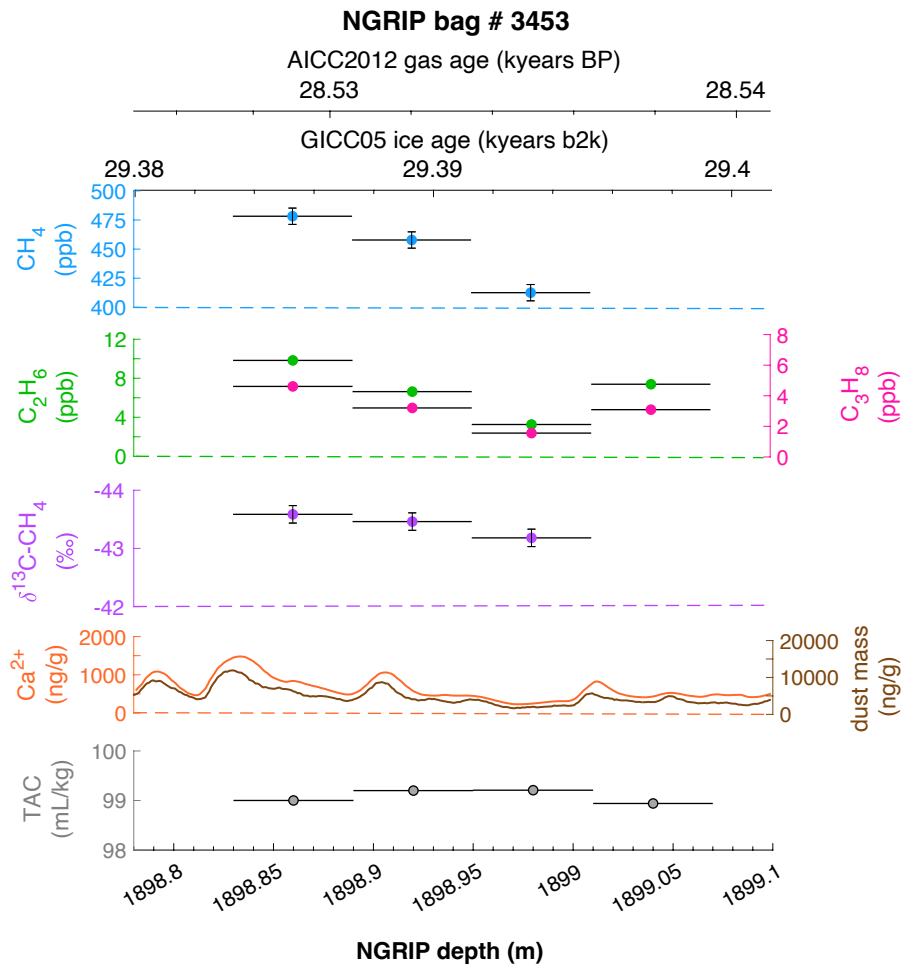
1239
1240
1241
1242
1243
1244
1245

Figure A2: **Detailed data overview for NGRIP bag 3453.** Bag-specific overview of parameters measured for each sample in this bag: methane, ethane, propane, $Ca^{2+}$, mineral dust mass, TAC (Total Air Content), $\delta^{13}C$-$CH_4$, indicated at the NGRIP depth (bottom axis) and the AICC2012 gas age (upper top axis) and the GICC05 ice age (lower top axis). The mineral dust record is taken from Ruth et al. (2003), the $Ca^{2+}$ record from Erhardt et al. (2022).
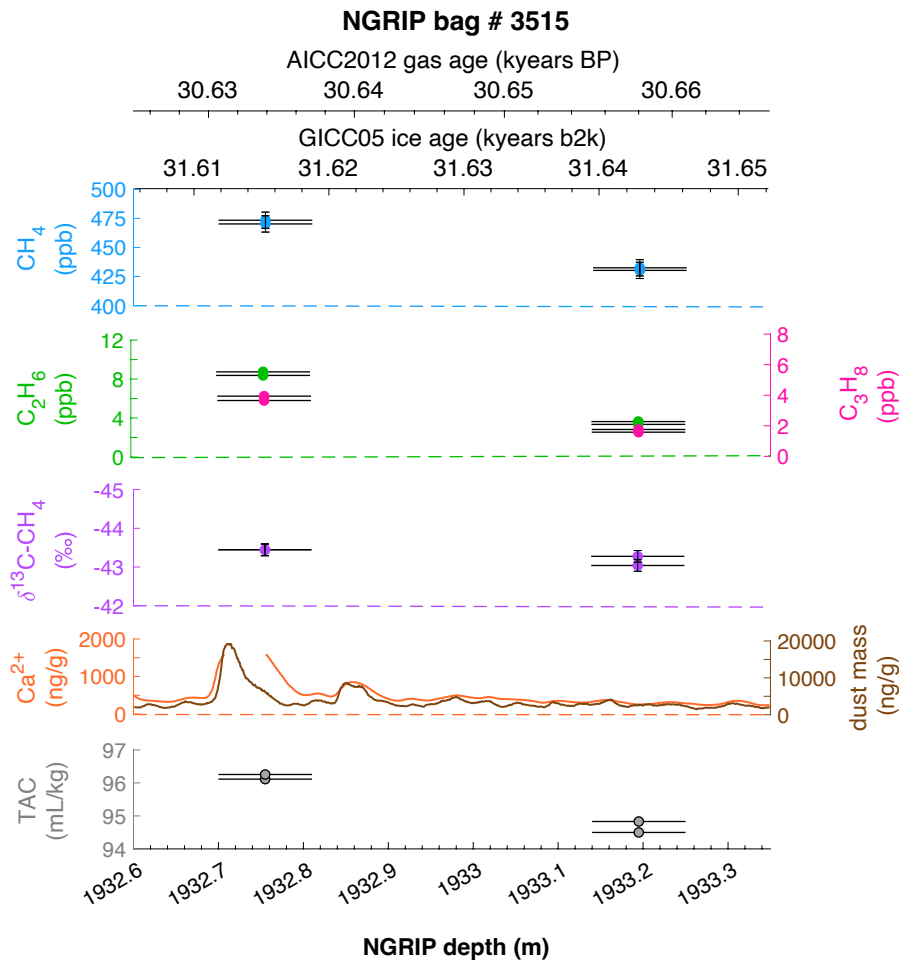
Figure A3: **Detailed data overview for NGRIP bag 3515.** Bag-specific overview of parameters measured for each sample in this bag: methane, ethane, propane, $Ca^{2+}$, mineral dust mass, TAC (Total Air Content), $\delta^{13}C$-$CH_4$, indicated at the NGRIP depth (bottom axis) and the AICC2012 gas age (upper top axis) and the GICC05 ice age (lower top axis). The mineral dust record is taken from Ruth et al. (2003), the $Ca^{2+}$ record from Erhardt et al. (2022). Note that there is a gap in the $Ca^{2+}$ record which was corrected by a fill routine for the analysis of the two measured samples at this depth.

1278    **Appendix B**

1279
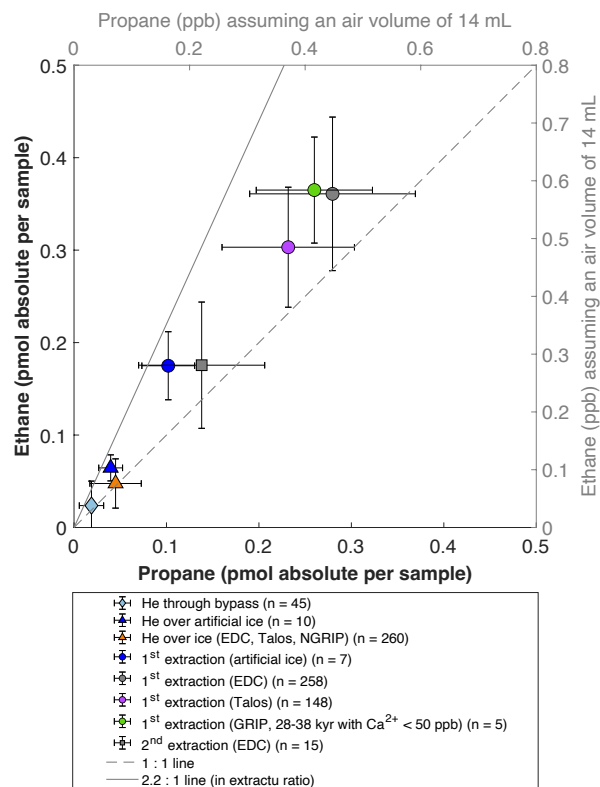
1280

1281    Figure B1: **Collection of different measurement modes and ice core sample locations to estimate individual**
1282    **blank contributions.** The mode "He through bypass" (diamond) refers to a measurement type where helium is
1283    injected into our system but without flowing through our extraction vessel. "He over ice" (triangles) refers to
1284    helium injections over the unmelted ice core sample. Results from the 1st extraction are shown for different ice
1285    cores (artificial gas-free ice, Talos Dome, EDC, GRIP; colored circles). The 2nd extraction of the Antarctic EDC
1286    ice core is marked as grey square. Lines with ethane/propane ratios are for orientation only.

1287

1288    In this section we provide background information of how we determined the blank

1289    contributions for our alkane measurements for the different measurement modes. Overall, our

1290    strategy is similar to the measurements which were published earlier in 2014 (Schmitt et al.,

1291    2014). Here we include more measurements performed since then with our $\delta^{13}$C-CH$_4$ device.

1292    Following the classic usage, blank contributions are related to the measurement device itself

1293    rather than to the sample, thus we report the measured values of the species as absolute amount

1294    in pmol with respect to a measurement procedure (sample run). To compare these absolute

1295    values with the classic units of species concentration in the air for an ice sample in ppb, Fig.

1296    B1 has secondary axes (grey) for the species concentrations in ppb for an assumed sample size

1297    of air of 14 mL STP (our typical ice core sample size).

1298    Since our extraction device is at vacuum conditions, a blank contribution from leaks that allow

1299    ambient air with relatively high ethane and propane concentrations to be collected together with

1300    our sample seems the most straightforward risk. To quantify this leak contribution, we routinely

1301 perform so called "He over ice" runs where a helium flow is passed over the unmelted ice core

1302 sample and the species are trapped on the cold activated carbon trap (see details in Schmitt et

1303 al., 2014). The trapping duration is the same as for the 1$^{st}$ extraction, thus this "He over ice"

1304 run mimics the contribution for the 1$^{st}$ extraction. As can be seen in Fig. B1, for ethane this

1305 "leak contribution" is typically <0.1 ppb, thus small compared to concentrations we see for

1306 dust-rich Greenland ice samples with about 6 ppb (see Fig. 5). However, this "He over ice"

1307 does not capture the actual melting process of the ice sample and represents the lowest blank

1308 boundary for our ice core samples. To mimic the full procedure an ice core samples experiences,

1309 we run a limited number of artificial gas-free ice samples (blue circles in Fig. B1). The ethane

1310 values obtained for these artificial ice sample is around 0.3 ppb and thus considerably higher

1311 than for the procedure without melting. This indicates that the presence of liquid water may

1312 lead to a desorption or production of alkanes from the inner walls of our extraction vessel.

1313 Alternatively, our artificial ice still contains traces of alkanes. So far, we could not solve this

1314 issue and more experiments are needed. A much larger data set on the upper boundary of the

1315 extraction blank comes from routine measurements of Antarctic ice core samples with the

1316 primary target of stable isotope analyses of $CH_4$ and $N_2O$. These Antarctic samples cover glacial

1317 and interglacial time intervals and the measured ethane values are typically around 0.55 ppb.

1318 Since the reconstructed atmospheric background for ethane in Antarctic ice is lower with values

1319 in the range of 0.1 – 0.15 ppb for the late Holocene (Nicewonger et al., 2018), a realistic blank

1320 contribution for our 1$^{st}$ extraction is on the order of 0.4 to 0.5 ppb. An additional constraint

1321 comes from five stadial GRIP samples from the time interval 28-38 kyears (green circle in Fig.

1322 B1) that have very low $Ca^{2+}$ content (< 50 ppb) and thus have likely a negligible contribution

1323 from a dust-related *in extractu* component. The measured ethane concentration from these

1324 GRIP samples is very similar to the Antarctic ice core samples. One possible explanation would

1325 be that the atmospheric ethane concentration during the glacial was similar and low for both

1326 hemispheres. Regardless of the individual contributions, for our considerations of dust-related

1327 *in extractu* production in Greenland ice cores the upper estimate for the sum of atmospheric

1328 background and blank contribution is about 0.55 ppb (about 0.35 pmol) for ethane. Since the

1329 ethane to propane ratio for these non-dust contributions is about 1.5, the corresponding propane

1330 values are lower by that value. Importantly, since the ethane to propane ratio for our dust-related

1331 production is with 2.2 rather similar, its impact on the calculated ethane to propane ratio (e.g.

1332 Fig. 4) is very minor and small within the error estimate. For that reason, we did not correct our

1333 Greenland measurements for any blank contribution and showed the values as measured along

1334 with measurements of Antarctic ice cores samples which serve as first-order blank estimates.

1335 **Appendix C**

1336
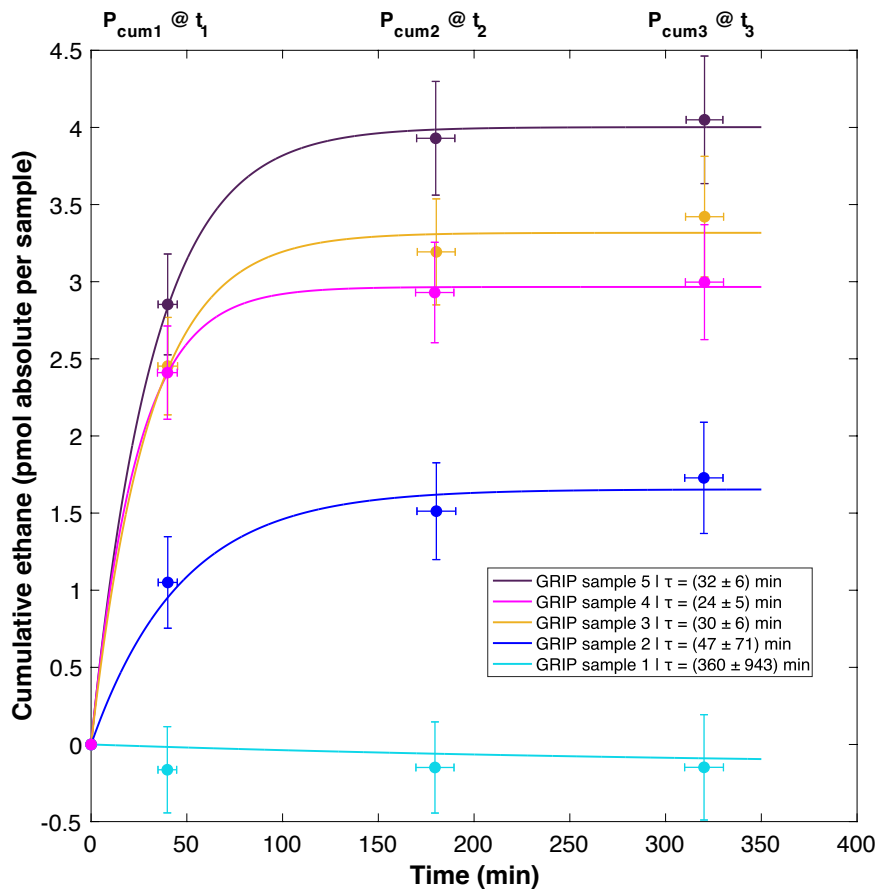
1337

1338

1339 Figure C1: **Temporal dynamics of excess ethane production in GRIP ice core samples.** Cumulative ethane
1340 amount from the 1st, 2nd, and 3rd extraction in relation to the time available for a potential reaction in the meltwater
1341 during each extraction. We assume a first-order reaction kinetic as model for our observations where the mean
1342 half-life time ($\tau$) and standard deviations are calculated for each GRIP sample from the compilation of all 1000
1343 iterations of our Monte Carlo approach. The numbered samples can also be found in Fig. 7a.

1344

1345 The general equation to describe a first-order chemical reaction or exponential decay process

1346 (e.g. release of adsorbed gas from the adsorbent) is Eqn. (1).

1347

1348 $N(t) = N_0 * e(-t/\tau)$ (1)

1349

1350 With $N_0$ being the total amount of substance (reactant) at the start of the reaction. N(t) equals

1351 the remaining amount of the reactant at time t, and t being time of reaction and $\tau$, the mean

1352 lifetime of the reaction. In our case, we cannot determine N(t) neither do we know $N_0$ but we

1353 experimentally determined the cumulative amount of the product, $P_{cum(t)}$, at three different times

1354 as our observable quantity. Thus, in Eqn. 2 we define $P_{cum(t)}$ as the difference between $N_0$ and

1355 N(t).

1356

1357     $P_{cum(t)} = N_0 - N(t)$                (2)

1358

1359 Replacing N(t) in Eqn. 1 with our definition in Eqn. 2 we obtain Eqn. 3, which contains two fit

1360 parameters, $N_0$ and $\tau$, as well as our observable parameter $P_{cum(t)}$, i.e. the cumulative amount of

1361 alkane for a certain time step.

1362

1363     $P_{cum(t)} = N_0 - N_0 * e(-t/\tau)$          (3)

1364

1365 For the five GRIP samples we have three consecutive measurements each, the 1st, 2nd, and 3rd

1366 extraction. The time-dependent $P_{cum(t)}$ values are as follows: $P_{cum0}$ is defined as 0, representing

1367 the state of the unmelted ice sample before liquid water is present. $P_{cum1}$ is the measured amount

1368 from the 1st extraction (ice extraction) minus the estimated contribution from the atmosphere

1369 and minus the blank contribution for the 1st extraction. $P_{cum2}$ is the sum of $P_{cum1}$ and the value

1370 from the 2nd extraction minus the blank contribution of the 2nd extraction. Similarly, $P_{cum3}$ is the

1371 sum of $P_{cum2}$ and the value from the 3rd extraction minus the blank for the 3rd extraction.

1372 To account for the uncertainties of the involved measurements and corrections, we added

1373 normally distributed errors to the following parameters (measured value ± 5 %; blank ± 20 %;

1374 atmospheric contribution ± 50 %), and we also assigned an uncertainty of 5 min to the time to

1375 account for variations of the melting speed of the ice and delays between the individual

1376 measurements (1st, 2nd, 3rd).

1377 For the fitting procedure we used the Matlab built in nonlinear least-squares solver called

1378 'lsqcurvefit' and performed 1000 runs where we varied the above-mentioned input parameters.

1379 The output of the function are the two fit parameters, i.e., $N_0$ and $\tau$. From the 1000 runs we

1380 calculated the mean and the 1 sigma standard deviation of the lifetime.

1381

1382 Note, this approach can only be suitably applied to ethane and propane as the past atmospheric

1383 contribution for these gases in the 1st extraction is typically small against the excess contribution

1384 for dust-rich samples. For our five GRIP samples, where we have three consecutive extractions,

1385 four samples are considered "dust-rich" and are suitable to provide robust estimates for $\tau$. In

1386 contrast, one sample is from an interstadial period with very low dust content and thus shows

1387 negligible production of alkanes in all three extractions. While this sample is not suited to

1388 provide robust estimates for $\tau$, this sample allows to assess the first-order plausibility of the

1389 blank correction and the assumed atmospheric background for ethane for the 1st extraction

1390 (sample number 1, bottom-most sample). For a sample without any *in extractu* production, the
1391 cumulative curve should be flat at around 0 which is the case within our error estimates.
1392
1393
1394

**Code availability**

1396 No special code related to the manuscript.
1397

**Data availability**

1399 Data is provided on request to the authors.
1400

**Author contribution**

1402 The experimental approach was defined by JS, HF and MM. MM and BS performed the
1403 measurements; MM and JS analyzed the data; MM wrote the manuscript draft; MM prepared
1404 the manuscript with contributions from all co-authors.
1405

**Competing interests**

1407 The authors declare that they have no conflict of interest.
1408

**Disclaimer**

1410 None.
1411

**Special issue statement**

1413 Ice core science at the three poles (CP/TC inter-journal SI)
1414

**Acknowledgments**

1416 We thank Murat Aydin for very helpful review comments. The research leading to these results
1417 has received funding from the Swiss National Science Foundation (no. 200020_172506 &
1418 200020B_200328). This work is a contribution to the NorthGRIP ice core project, which is
1419 directed and organized by the Department of Geophysics at the Niels Bohr Institute for
1420 Astronomy, Physics and Geophysics, University of Copenhagen. It is supported by funding
1421 agencies in Denmark (SNF), Belgium (FNRS-CFB), France (IFRTP and NSU/CNRS),
1422 Germany (AWI), Iceland (RannIs), Japan (MEXT), Sweden (SPRS), Switzerland (SNF), and
1423 the United States (NSF).

**References**

Althoff, F., Jugold, A. and Keppler, F.: Methane formation by oxidation of ascorbic acid using iron minerals and hydrogen peroxide. Chemosphere 80, 286–292, https://doi.org/10.1016/j.chemosphere.2010.04.004, 2010

Althoff, F., Benzing, K., Comba, P., McRoberts, C., Boyd, D. R., Greiner, S. and Keppler, F.: Abiotic methanogenesis from organosulphur compounds under ambient conditions, Nat Commun, 5, 4205, https://doi.org/10.1038/ncomms5205, 2014

Anklin, M., Barnola, J.-M., Schwander, J., Stauffer, B., and Raynaud, D.: Processes affecting the $CO_2$ concentrations measured in Greenland ice, Tellus, 47, 461-470, https://doi.org/10.1034/j.1600-0889.47.issue4.6.x, 1995

Apel, K. and Hirt, H.: Reactive Oxygen Species: Metabolism, Oxidative Stress, and Signal Transduction, Annual Review of Plant Biology 2004, 55:1, 373-399, https://doi.org/10.1146/annurev.arplant.55.031903.141701, 2004

Austin, A. T., Méndez, M. S., and Ballaré, C. L.: Photodegradation alleviates the lignin bottleneck for carbon turnover in terrestrial ecosystems, PNAS, 13 (16), 4392-4397, https://doi.org/10.1073/pnas.1516157113, 2016

Baumgartner, M., Schilt, A., Eicher, O., Schmitt, J., Schwander, J., Spahni, R., Fischer, H., and Stocker, T. F.: High-resolution interpolar difference of atmospheric methane around the Last Glacial Maximum, Biogeosciences, 9, 3961–3977, https://doi.org/10.5194/bg-9-3961-2012, 2012

Baumgartner, M., Kindler, P., Eicher, O., Floch, G., Schilt, A., Schwander, J., Spahni, R., Capron, E., Chappellaz, J., Leuenberger, M., Fischer, H., and Stocker, T. F.: NGRIP $CH_4$ concentration from 120 to 10 kyr before present and its relation to a $\delta^{15}N$ temperature reconstruction from the same ice core, Clim. Past, 10, 903–920, https://doi.org/10.5194/cp-10-903-2014, 2014

Beck, J., Bock, M., Schmitt, J., Seth, B., Blunier, T., and Fischer, H.: Bipolar carbon and hydrogen isotope constraints on the Holocene methane budget, Biogeosciences, 15, 7155–7175, https://doi.org/10.5194/bg-15-7155-2018, 2018

Bernard, B., Brooks, J.M. and Sackett, W.M.: A geochemical model for characterization of hydrocarbon gas sources in marine sediments. In: 9th Annual Offshore Technology Conference, Houston, Texas, May 1977, 435–438 (OTC 2934), https://doi.org/10.4043/2934-MS, 1977

Biscaye, P. E., Grousset, F. E., Revel, M., Van der Gaast, S., Zielinski, G. A., Vaars, A. and G. Kukla: Asian provenance of Glacial dust (stage 2) in the Greenland Ice Sheet Project 2 Ice Core, Summit, Greenland, J. Geophys. Res., 102, 26,765-26,781, 1997

Bock, M., Schmitt, J., Behrens, M., Möller, L., Schneider, R., Sapart, C. and Fischer, H.: A gas chromatography/pyrolysis/isotope ratio mass spectrometry system for high- precision dD measurements of atmospheric methane extracted from ice cores, Rapid Commun. Mass Spectrom, 24, 621–633, https://doi.org/10.1002/rcm.4429, 2010a

Bock, M., Schmitt, J., Blunier, T., Fischer, H., Möller, L. and Spahni, R.: Hydrogen Isotopes Preclude Marine Hydrate CH4 Emissions at the Onset of Dansgaard- Oeschger Events, Science, 328, 1686-1689, https://doi.org/10.1126/science.1187651, 2010b

Bock, M., Schmitt, J., Beck, J., Schneider, R., and Fischer, H.: Improving accuracy and precision of ice core $\delta D(CH_4)$ analyses using methane pre-pyrolysis and hydrogen post-pyrolysis trapping and subsequent chromatographic separation, Atmos. Meas. Tech., 7, 1999–2012, https://doi.org/10.5194/amt-7-1999-2014, 2014

Bock, M., Schmitt, J., Beck, J., Seth, B., Chappellaz, J. and Fischer, H.: Glacial/ interglacial wetland, biomass burning, and geologic methane emissions constrained by dual stable isotopic CH4 ice core records, PNAS, 114 (29), E5778-E5786, https://doi.org/10.1073/pnas.1613883114, 2017

Bruhn, D., Mikkelsen, T. N., Øbro, J., Willats, W. G. T. and Ambus, P.: Effects of temperature, ultraviolet radiation and pectin methyl esterase on aerobic methane release from plant material, Plant Biology, 11, 43-48, https://doi.org/10.1111/j.1438-8677.2009.00202.x, 2009

Campen, R. K., Sowers, T., and Alley, R. B.: Evidence of microbial consortia metabolizing within a low-latitude mountain glacier, Geology, 31, 231–234, https://doi.org/10.1130/0091-7613(2003)031<0231:EOMCMW>2.0.CO;2, 2003

Chappellaz, J., Blunier, T., Kints, S., Dällenbach, A., Barnola, J. M., Schwander, J., Raynaud, D. and Stauffer B.: Changes in the atmospheric CH4 gradient between Greenland and Antarctica during the Holocene, Geophys. Res. Let., Volume 102, 15987-15997, https://doi.org/10.1029/97JD01017,1997

Cheng, A.-L. and Huang, W.-L.: Selective adsorption of hydrocarbon gases on clays and organic matter, Org. Geochem., 35, 413-423, https://doi.org/10.1016/j.orggeochem.2004.01.007, 2004

Dan, J., Kumai, T., Sugimoto, A. and Murase, J.: Biotic and abiotic methane releases from Lake Biwa sediment slurry, Limnology 5, 149–154, https://doi.org/10.1007/s10201-004-0124-7, 2004

Derendorp, L., Holzinger, R., Wishkerman, A., Keppler, F., and Röckmann, T.: VOC emissions from dry leaf litter and their dependence on temperature, Biogeosciences Discuss., 7, 823–854, https://doi.org/10.5194/bgd-7-823-2010, 2010

Derendorp, L., Holzinger, R., Wishkerman, A., Keppler, F., and Röckmann, T.: Methyl chloride and C2-C5 hydrocarbon emissions from dry leaf litter and their dependence on temperature, Atmospheric Environment, 45, 3112-3119, https://doi.org/10.1016/j.atmosenv.2011.03.016, 2011

Dumelin, E.E. and Tappel, A.L.: Hydrocarbon gases produced during in vitro peroxidation of polyunsaturated fatty acids and decomposition of preformed hydroperoxides, Lipids, 12, 894, https://doi.org/10.1007/BF02533308, 1977

Dyonisius, M. N., Petrenko, V. V., Smith, A.M., Hua, Q., Yang, B., Schmitt, J., Beck, J., Seth, B., Bock, M., Hmiel, B., Vimont, I., Menking, J. A., Shackleton, S. A., Baggenstos, D.,

1526    Bauska, T. K., Rhodes, R., Sperlich, P., Beaudette, R., Harth, C., Kalk, M., Brook, E. J.,
1527    Fischer, H., Severinghaus, J. P. and Weiss, R. F.: Old carbon reservoirs were not important in
1528    the deglacial methane budget, Science, 367(6480), 907-910,
1529    https://doi.org/10.1126/science.aax0504, 2020
1530
1531    Erhardt, T., Bigler, M., Federer, U., Gfeller, G., Leuenberger, D., Stowasser, O.,
1532    Röthlisberger, R., Schüpbach, S., Ruth, U., Twarloh, B., Wegner, A., Goto-Azuma, K.,
1533    Kuramoto, T., Kjær, H. A., Vallelonga, P. T., Siggaard-Andersen, M.-L., Hansson, M. E.,
1534    Benton, A. K., Fleet, L. G., Mulvaney, R., Thomas, E. R., Abram, N., Stocker, T. F., and
1535    Fischer, H.: High resolution aerosol concentration data from the Greenland NorthGRIP and
1536    NEEM deep ice cores, Earth Syst. Sci. Data Discuss., 14, 1215–1231,
1537    https://doi.org/10.5194/essd-14-1215, 2022
1538
1539    Etiope, G. and Klusman, R. W.: Geologic emissions of methane to the atmosphere,
1540    Chemosphere, 49, 8, 777-789, https://doi.org/10.1016/S0045-6535(02)00380-6, 2002
1541
1542    Etiope G., Martinelli G., Caracausi, A. and Italiano, F.: Methane seeps and mud volcanoes in
1543    Italy: gas origin, fractionation and emission to the atmosphere, Geophys. Res. Lett., 34,
1544    https://doi.org/10.1029/2007GL030341, 2007
1545
1546    Etiope G., Lassey K. R., Klusman R. W. and Boschi, E.: Reappraisal of the fossil methane
1547    budget and related emission from geologic sources, Geophys. Res. Lett., 35,
1548    https://doi.org/10.1029/2008GL033623, 2008
1549
1550    Frahry, G. and Schopfer, P.: Hydrogen peroxide production by roots and its stimulation by
1551    exogenous NADH, Physiologia Plantarum, 103, 395-404, https://doi.org/10.1034/j.1399-
1552    3054.1998.1030313.x, 1998
1553
1554    Flückiger J., Blunier T., Stauffer B., Chappellaz M., Spahni R., Kawamura K., Schwander J.,
1555    Stocker T. F. and Dahl-Jensen, D.: N2O and CH4 variations during the last glacial epoch:
1556    Insight into global processes, Global Biogeochem. Cy 18, 1020,
1557    https://doi.org/10.1029/2003GB002122, 2004
1558
1559    Fuhrer, K. and Legrand, M.: Continental biogenic species in the Greenland Ice Core Project
1560    ice core: Tracing back the biomass history of the North American continent, J. Geophys. Res.,
1561    102(C12), 26735– 26745, https://doi.org/10.1029/97JC01299, 1997
1562
1563    Georgiou, C. D., Sun, H. J., McKay, C. P., Grintzalis, K., Papapostolou, I., Zisimopoulos, D.,
1564    Panagiotidis, K., Zhang, G., Koutsopoulou, E., Christidis, G. E. and Margiolaki, I.: Evidence
1565    for photochemical production of reactive oxygen species in desert soils, Nat.
1566    Commun., 6, 7100, https://doi.org/10.1038/ncomms8100, 2015
1567
1568    Giorio, C., Kehrwald, N., Barbante, C., Kalberer, M., King, A. C. F., Thomas, E. R., Wolff,
1569    E. W. and Zennaro, P.: Prospects for reconstructing paleoenvironmental conditions from
1570    organic compounds in polar snow and ice, Quaternary Science Reviews, 183, 1-22,
1571    https://doi.org/10.1016/j.quascirev.2018.01.007, 2018
1572
1573    Han, C., Do Hur, S., Han, Y., Lee, K., Hong, S., Erhard, T., Fischer, H., Svensson, A. M.,
1574    Steffensen, J. P. and Vallelonga, P.: High-resolution isotopic evidence for a potential Saharan
1575    provenance of Greenland glacial dust. Sci Rep 8, 15582, https://doi.org/10.1038/s41598-018-
1576    33859-0, 2018

1577
1578 Harris, E., Sinha, B., van Pinxteren, D., Tilgner, A., Wadinga Fomba, K., Schneider, J., Roth,
1579 A., Gnauk, T., Fahlbusch, B., Mertes, S., Lee, T., Collett, J., Foley, S., Borrmann, S., Hoppe,
1580 P. and Herrmann, H.: Enhanced Role of Transition Metal Ion Catalysis During In-Cloud
1581 Oxidation of $SO_2$, *Science,* 340, 727-730, https://doi.org:doi:10.1126/science.1230911, 2013
1582
1583 Helmig, D., Petrenko, V., Martinerie, P., Witrant, E., Röckmann, T., Zuiderweg, A.,
1584 Holzinger, R., Hueber, J., Thompson, C., White, J. W. C., Sturges, W., Baker, A., Blunier, T.,
1585 Etheridge, D., Rubino, M., and Tans, P.: Reconstruction of Northern Hemisphere 1950–2010
1586 atmospheric non-methane hydrocarbons, Atmos. Chem. Phys., 14, 1463-1483,
1587 https://doi.org/10.5194/acp-14-1463, 2014
1588
1589 Hoheisel, A., Yeman, C., Dinger, F., Eckhardt, H., and Schmidt, M.: An improved method for
1590 mobile characterisation of $\delta^{13}CH_4$ source signatures and its application in Germany, Atmos.
1591 Meas. Tech., 12, 1123–1139, https://doi.org/10.5194/amt-12-1123-2019, 2019.
1592
1593 Hurkuck, M., Althoff, F., Jungkunst, H. F., Jugold, A. and Keppler, F.: Release of methane
1594 from aerobic soil: An indication of a novel chemical natural process?, Chemosphere, 86, 684-
1595 689, https://doi.org/10.1016/j.chemosphere.2011.11.024, 2012
1596
1597 Ji, L., Zhang, T., Milliken, K. L., Qu, J. and Zhang, X.: Experimental investigation of main
1598 controls to methane adsorption in clay-rich rocks, Appl. Geochem. 27, 2533–2545,
1599 https://doi.org/10.1016/j.apgeochem.2012.08.027, 2012
1600
1601 John, W. W. and Curtis, R. W.: Isolation and Identification of the Precursor of Ethane
1602 in Phaseolus vulgaris L., Plant Physiology, 59, 521–522, https://doi.org/10.1104/pp.59.3.521,
1603 1977
1604
1605 Jugold, A., Althoff, F., Hurkuck, M., Greule, M., Lenhart, K., Lelieveld, J., and Keppler, F.:
1606 Non-microbial methane formation in oxic soils, Biogeosciences, 9, 5291–5301,
1607 https://doi.org/10.5194/bg-9-5291-2012, 2012
1608
1609 Katagi, T.: Photoinduced Oxidation of the organophosphorus Fungicide Tolclofs-methyl on
1610 Clay Minerals, J. Agrie. Food Cham., 38, 1595-1600, 1990
1611
1612 Kaufmann, P. R., Federer, U., Hutterli, M. A., Bigler, M., Schüpbach, S., Ruth, U., Schmitt, J.
1613 and Stocker, T. F.: An Improved Continuous Flow Analysis System for High-Resolution
1614 Field Measurements on Ice Cores, Environmental Science & Technology, 42 (21), 8044-
1615 8050, https://doi.org/10.1021/es8007722, 2008
1616
1617 Keeling, C. D.: The concentration and isotopic abundance of carbon dioxide in rural areas,
1618 Geochim. Cosmochim. Acta, 13, 322–334 https://doi.org/10.1016/0016-7037(58)90033-
1619 4.1958, 1958
1620
1621 Keeling, C. D.: The concentration and isotopic abundance of carbon dioxide in rural and
1622 marine air, Geochim. Cosmochim. Acta, 24, 277–298, https://doi.org/10.1016/0016-
1623 7037(61)90023-0, 1961
1624
1625 Keppler, F., Hamilton, J. T. G., Braß, M. and Röckmann, T.: Methane emissions from
1626 terrestrial plants under aerobic conditions, Nature 439, 187–191,
1627 https://doi.org/10.1038/nature04420, 2006

1628

1629 Keppler, F., Hamilton, J. T. G., McRoberts, W. C., Vigano, I., Braß, M. and Röckmann, T.:
1630 Methoxyl groups of plant pectin as a precursor of atmospheric methane: evidence from
1631 deuterium labelling studies, New Phytologist, 178, 808-814, https://doi.org/10.1111/j.1469-
1632 8137.2008.02411.x, 2008

1633

1634 Kibanova, D., Trejo, M., Destaillats, H. and Cervini-Silva, J.: Photocatalytic activity of
1635 kaolinite, Catalysis Communications, 12, 698-702,
1636 https://doi.org/10.1016/j.catcom.2010.10.029, 2011

1637

1638 Köhler, P., Fischer, H., Schmitt, J., and Munhoven, G.: On the application and interpretation
1639 of Keeling plots in paleo climate research – deciphering $\delta^{13}C$ of atmospheric $CO_2$ measured in
1640 ice cores, Biogeosciences, 3, 539–556, https://doi.org/10.5194/bg-3-539-2006, 2006

1641

1642 Lee, L. E., Edwards, J. S., Schmitt, J., Fischer, H., Bock, M. and Brook, E. J.: Excess methane
1643 in Greenland ice cores associated with high dust concentrations, Geochim. Cosmochim. Acta,
1644 270, 409-430, https://doi.org/10.1016/j.gca.2019.11.020, 2020

1645

1646 Legrand, M., and Delmas, R.: Soluble Impurities in Four Antarctic Ice Cores Over the Last
1647 30000 Years, Annals of Glaciology, 10, 116-120,
1648 https://doi.org/10.3189/S0260305500004274, 1988

1649

1650 Liu, J., Chen, H., Zhu, Q., Shen, Y., Wang, X., Wang, M., Peng, C.: A novel pathway of
1651 direct methane production and emission by eukaryotes including plants, animals and fungi:
1652 An overview, Atmospheric Environment, 115, 26,
1653 https://doi.org/10.1016/j.atmosenv.2015.05.019, 2015

1654

1655 Liu, D., Yuan, P., Liu, H., Li, T., Tan, D., Yuan, W., He, H.: High-pressure adsorption of
1656 methane on montmorillonite, kaolinite and illite, Applied Clay Science,85, 25-30,
1657 https://doi.org/10.1016/j.clay.2013.09.009, 2013

1658

1659 Lupker, M., Aciego, S. M., Bourdon, B., Schwander, J., and Stocker, T. F.: Isotopic tracing
1660 (Sr, Nd, U and Hf) of continental and marine aerosols in an 18th century section of the Dye-3
1661 ice core (Greenland), Earth Pla Sci Let, 295, 277-286,
1662 https://doi.org/10.1016/j.epsl.2010.04.010, 2010

1663

1664 McLeod, A. R., Newsham, K. K. and Fry, S.C.: Elevated UV-B radiation modifies the
1665 extractability of carbohydrates from leaf litter of Quercus robur, Soil Biology and
1666 Biochemistry, 39, Issue 1, 116-126, https://doi.org/10.1016/j.soilbio.2006.06.019, 2007

1667

1668 McLeod, A.R., Fry, S.C., Loake, G.J., Messenger, D.J., Reay, D.S., Smith, K.A. and Yun, B.-
1669 W.: Ultraviolet radiation drives methane emissions from terrestrial plant pectins, New
1670 Phytologist, 180, 124-132, https://doi.org/10.1111/j.1469-8137.2008.02571.x, 2008

1671

1672 Messenger, D.J., McLeod, A. R. and Fry, S.C.: The role of ultraviolet radiation,
1673 photosensitizers, reactive oxygen species and ester groups in mechanisms of methane
1674 formation from pectin, Plant, Cell & Environment, 32: 1-9, https://doi.org/10.1111/j.1365-
1675 3040.2008.01892.x, 2009

1676

1677 Milkov, A. V. and Etiope, G.: Revised genetic diagrams for natural gases based on a global
1678 dataset of >20,000 samples, Organic Geochemistry, 125, 109-120,
1679 https://doi.org/10.1016/j.orggeochem.2018.09.002, 2018

1681 Mitchell, L., Brook, E., Lee, J. E., Buizert, C., and Sowers, T.: Constraints on the Late
1682 Holocene anthropogenic contribution to the atmospheric methane budget, Science 342, 964–
1683 966, https://doi.org/10.1126/science.1238920, 2013

1685 Miteva V., Teacher C., Sowers T. and Brenchley, J.: Comparison of the microbial diversity at
1686 different depths of the GISP2 Greenland ice core in relationship to deposition climates,
1687 Environ. Microbiol., 11, 640–656, https://doi.org/10.1111/j.1462-2920.2008.01835.x, 2009

1689 Möller, L., Sowers, T., Bock, M., Spahni, R., Behrens, M., Schmitt, J., Miller, H. and Fischer,
1690 H.: Independent variations of CH4 emissions and isotopic composition over the past 160,000
1691 years, Nature Geosci, 6, 885–890, https://doi.org/10.1038/ngeo1922, 2013

1693 Mohnen, D.: Pectin structure and biosynthesis, Current Opinion in Plant Biology, 11, 266-
1694 277, https://doi.org/10.1016/j.pbi.2008.03.006, 2008

1696 NEEM community members: Eemian interglacial reconstructed from a Greenland folded ice
1697 core, Nature, 493, 489–494, https://doi.org/10.1038/nature11789, 2013

1699 Nicewonger, M. R., Verhulst, K. R., Aydin, M. and Saltzman, E. S.: Preindustrial
1700 atmospheric ethane levels inferred from polar ice cores: A constraint on the geologic sources
1701 of atmospheric ethane and methane, Geophys. Res. Lett., 43,
1702 https://doi.org/10.1002/2015GL066854, 2016

1704 Nicewonger, M. R., Aydin, M., Prather, M. J., and Saltzman, E.S.: Large changes in biomass
1705 burning over the last millennium inferred from paleoatmospheric ethane in polar ice cores,
1706 Proc. Natl. Acad. Sci. USA, 115 (49), 12413-12418,
1707 https://doi.org/10.1073/pnas.1807172115, 2018

1709 North Greenland Ice Core Project members: High-resolution record of Northern Hemisphere
1710 climate extending into the last interglacial period, *Nature* 431, 147–151,
1711 https://doi.org/10.1038/nature02805, 2004

1713 Pires, J., Bestilleiro, M., Pinto, M. and Gil, A.: Selective adsorption of carbon dioxide,
1714 methane and ethane by porous clays heterostructures, Separation and Purification
1715 Technology, 61, 161-167, https://doi.org/10.1016/j.seppur.2007.10.007, 2008

1717 Price, P. B. and Sowers, T.: Temperature dependence of metabolic rates for microbial growth,
1718 maintenance, and survival, P. Natl. Acad. Sci. USA 101, 4631–4636,
1719 https://doi.org/10.1073/pnas.0400522101, 2004

1721 Qian, G., Chang, S. X., ZhiPing, W., JinChao, F., QuanSheng, C., XingGuo, H.: Microbial
1722 versus non-microbial methane releases from fresh soils at different temperatures, Geoderma,
1723 284, 178-184, https://doi.org/10.1016/j.geoderma.2016.08.027, 2016

1724
1725

1726 Rohde, R. A., Price, P. B., Bay, R. C. and Bramall, N. E.: In situ microbial metabolism as a
1727 cause of gas anomalies in ice, P. Natl. Acad. Sci. USA, 105, 8667–8672,
1728 https://doi.org/10.1073/pnas.0803763105, 2008

1729
1730 Rhodes, R. H., Faïn, X., Stowasser, C., Blunier, T., Chappellaz, C., McConnell, J. R.,
1731 Romanini, D., Mitchell, L. E. and Brook, E. J.: Continuous methane measurements from a
1732 late Holocene Greenland ice core: Atmospheric and in situ signals, Earth and Planetary
1733 Science Letters, 368, 9-19, https://doi.org/10.1016/j.epsl.2013.02.034, 2013

1734
1735 Rhodes, R. H., Faïn, X., Brook, E. J., McConnell, J. R., Maselli, O. J., Sigl, M., Edwards, J.,
1736 Buizert, C., Blunier, T., Chappellaz, J., and Freitag, J.: Local artifacts in ice core methane
1737 records caused by layered bubble trapping and in situ production: a multi-site investigation,
1738 Clim. Past, 12, 1061–1077, https://doi.org/10.5194/cp-12-1061-2016, 2016

1739
1740 Ross, D. J. K. and Bustin, R. M.: The importance of shale composition and pore structure
1741 upon gas storage potential of shale gas reservoirs, Mar. Petrol. Geol., 26, 916-927,
1742 https://doi.org/10.1016/j.marpetgeo.2008.06.004, 2009

1743
1744 Ruth, U., Wagenbach, D., Steffensen, J. P. and Bigler, M.: Continuous record of microparticle
1745 concentration and size distribution in the central Greenland NGRIP ice core during the last
1746 glacial period, J. Geophys. Res., 108 (D3), 4098, https://doi.org/10.1029/2002JD002376,
1747 2003

1748
1749 Ruth, U., Bigler, M., Röthlisberger, R., Siggaard-Andersen, M.-L., Kipfstuhl, S., Goto-
1750 Azuma, K., Hansson, M. E., Johnsen, S. J., Lu, H., and Steffensen, J. P.: Ice core evidence
1751 for a very tight link between North Atlantic and east Asian glacial climate, *Geophys. Res.*
1752 *Lett.*, 34, L03706, doi:10.1029/2006GL027876, 2007

1753
1754 Schade, G. W., Hofmann, R.-M. and Crutzen, P. J.: CO emissions from degrading plant
1755 matter, Tellus B: Chemical and Physical Meteorology, 51:5, 889-908,
1756 https://doi.org/10.3402/tellusb.v51i5.16501, 1999

1757
1758 Schilt, A., Baumgartner, M., Blunier, T., Schwander, J., Spahni, R., Fischer, H., and Stocker,
1759 T. F.: Glacial–interglacial and millennial-scale variations in the atmospheric nitrous oxide
1760 concentration during the last 800,000 years, Quat Sci Rev, 29, 182-192,
1761 https://doi.org/10.1016/j.quascirev.2009.03.011, 2010

1762
1763 Schmitt, J., Seth, B., Bock, M. and Fischer, H.: Online technique for isotope and mixing ratios
1764 of CH4, N2O, Xe and mixing ratios of organic trace gases on a single ice core sample, Atmos.
1765 Meas. Tech., 7, 2645–2665, https://doi.org/10.5194/amt-7-2645-2014, 2014

1766
1767 Smith, H. J., Wahlen, M., Mastroianni, D., and Taylor, K. C.: The $CO_2$ concentration of air
1768 trapped in GISP2 ice from the Last Glacial Maximum-Holocene transition, Geophys Res Let,
1769 24, 1-4, https://doi.org/10.1029/96GL03700, 1997

1770
1771 Sugimoto, A., Dan, J., Kumai, T. and Murase, J.: Adsorption as a methane storage process in
1772 natural lake sediment, Geophys. Res. Lett. 30, 2080, https://doi.org/10.1029/2003GL018162,
1773 2003
1774

Svensson, A., Biscaye, P. E. and Grousset, F. E.: Characterization of late glacial continental dust in the Greenland Ice Core Project ice core, J. Geophys. Res.-Atmos., 105, 4637–4656, https://doi.org/10.1029/1999JD901093, 2000

Tian, Y., Yan, C. and Jin, Z.: Characterization of Methane Excess and Absolute Adsorption in Various Clay Nanopores from Molecular Simulation, Sci Rep 7, 12040, https://doi.org/10.1038/s41598-017-12123, 2017

Tung, H. C., Bramall, N. E. and Price, P. B.: Microbial origin of excess methane in glacial ice and implications for life on Mars, P. Natl. Acad. Sci. USA 102, 18292–18296, https://doi.org/10.1073/pnas.0507601102, 2005

Tung, H., Price, P., Bramall, N. and Vrdoljak G.: Microorganisms metabolizing on clay grains in 3-km-deep Greenland basal ice, Astrobiology 6, 69–86. https://doi.org/10.1089/ast.2006.6.69, 2006

Vigano, I., van Weelden, H., Holzinger, R., Keppler, F., McLeod, A., and Röckmann, T.: Effect of UV radiation and temperature on the emission of methane from plant biomass and structural components, Biogeosciences, 5, 937–947, https://doi.org/10.5194/bg-5-937-2008, 2008

Vigano, I., Röckmann, T., Holzinger, R., van Dijk, A., Keppler, F., Greule, M., Brand, W. A., Geilmann, H. and van Weelden, H.: The stable isotope signature of methane emitted from plant material under UV irradiation, Atmospheric Environment, 43, 5637-5646, https://doi.org/10.1016/j.atmosenv.2009.07.046, 2009

Vigano, I., Holzinger, R., Keppler, F., Greule, M., Brand, W. A., Geilmann, H., van Weelden, H. and Röckmann, T.: Water drives the deuterium content of the methane emitted from plants, Geochimica et Cosmochimica Acta,74, 3865-3873, https://doi.org/10.1016/j.gca.2010.03.030, 2010

Wang, Z.-P., Han, X.-G., Wang, G. G., Song, Y. and Gulledge, J.: Aerobic methane emission from plants in the Inner Mongolia steppe, Environmental Science & Technology 42, 62– 68 https://doi.org/10.1021/es071224l, 2008

Wang, Z.-P., Xie, Z.-Q., Zhang, B.-C., Hou, L.-Y., Zhou, Y.-H., Li, L.-H. and Han, X.-G.: Aerobic and Anaerobic Nonmicrobial Methane Emissions from Plant Material, Environmental Science & Technology 2011 45 (22), 9531-9537, https://doi.org/10.1021/es2020132, 2011

Wang, B., Hou, L., Liu, W. and Wang, Z.: Non-microbial methane emissions from soils, Atmospheric Environment, 80, 290–298, https://doi.org/10.1016/j.atmosenv.2013.08.010, 2013

Wang, B., Lerdau, M. and He, Y.: Widespread production of nonmicrobial greenhouse gases in soils, Glob Change Biol., 23:4472–4482, https://doi.org/10.1111/gcb.13753, 2017

Watanabe, M., Watanabe, Y., Kim, Y. S., Koike, T.: Dark aerobic methane emission associated to leaf factors of two Acacia and five Eucalyptus species, Atmospheric Environment, 54, 277-281, https://doi.org/10.1016/j.atmosenv.2012.02.012, 2012

1826    Wehr, R. and Saleska, S. R.: The long-solved problem of the best-fit straight line: application
1827    to isotopic mixing lines, Biogeosciences, 14, 17–29, https://doi.org/10.5194/bg-14-17-2017,
1828    2017

1830    Whiticar, M. J.: Carbon and hydrogen isotope systematics of bacterial formation and
1831    oxidation of methane, Chemical Geology, 161, 291-314, https://doi.org/10.1016/S0009-
1832    2541(99)00092-3, 1999

1834    Wu, F., Li, J., Peng, Z., and Deng, N.: Photochemical formation of hydroxyl radicals
1835    catalyzed by montmorillonite, Chemosphere, 72, 407-413,
1836    https://doi.org/10.1016/j.chemosphere.2008.02.034, 2008

1838    York, D.: Least squares fitting of a straight line with correlated errors, Earth and Planetary
1839    Science Letters, 5, 320-324, https://doi.org/10.1016/S0012-821X(68)80059-7, 1968

1841    York, D., Evensen, N. M., Martınez, M. L., and De Basabe Delgado, J.: Unified equations for
1842    the slope, intercept, and standard errors of the best straight line, Am. J. Phys. 72, 367–375,
1843    https://doi.org/10.1119/1.1632486, 2004